Force Control of Heavy Lift Manipulators for High Precision Insertion Tasks

by

Matthew A. DiCicco

Bachelor of Science, Mechanical Engineering
Carnegie Mellon University, 2003

Submitted to the Department of Mechanical Engineering
in partial fulfillment of the requirements for the degree of
Masters of Science in Mechanical Engineering
at the
Massachusetts Institute of Technology

May 2005
[June 2005]

Signature of Author . . . . /. . . . .

Department of Mechanical Engineering
May 20, 2005

Certified by . . . .

Steven Dubowsky
Professor of Mechanical Engineering
Thesis Advisor

Accepted by . . . .

Professor Lallit Anand
Chairman, Committee on Graduate Studies
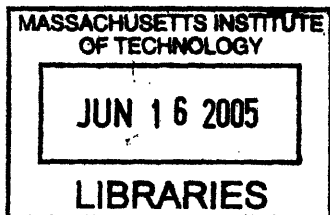
ARCHIVES

Force Control of Heavy Lift Manipulators for High Precision Insertion Tasks

by

Matthew A. DiCicco

Submitted to the Department of Mechanical Engineering
on May 6, 2005, in partial fulfillment of the
requirements for the degree of
Masters of Science in Mechanical Engineering

Abstract

The inherent strength of robotic manipulators can be used to assist humans in performing heavy lifting tasks. These robots reduce manpower, reduce fatigue, and increase productivity. This thesis deals with the development of a control system for a robot being built for this purpose. The task for this robot is to lift heavy payloads while performing complex insertion tasks. This task must be completed on the deck of a naval vessel where possible disturbances include wind, rain, poor visibility, and dynamic loads induced by a swaying deck.

The primary objective of the controller being designed here is to allow for insertion of the payload despite tight positioning tolerances and disturbances like surface friction, joint friction, and dynamic loads from ship motions. A control structure designed for intuitive interaction between the robot and operator is analyzed and shown to be stable using an established environment interaction model. The controller is shown to perform within established specifications via numerical simulation based on simple user inputs.

An additional objective of this controller design is to prevent part jamming during the insertion task. With a large, powerful manipulator, the chances of a jam occurring is high. Without the use of bilateral force feedback, it will be difficult for the operator feel when these jams will occur and there will be no information about how to prevent them. This thesis analyzes the geometry and mechanics of the jamming problem and derives a control system to assist the user in preventing these jams. These methods can be extended to other insertion tasks simply by specifying the appropriate geometry.

Thesis Supervisor: Steven Dubowsky, Professor of Mechanical Engineering

ACKNOWLEDGEMENTS

CONTENTS

FIGURES AND TABLES

Figures:

Tables:

CHAPTER

1

INTRODUCTION

1.1 Overview

This thesis describes the design of a control system for a large robotic manipulator for the United States Navy. This manipulator will be used aboard naval vessels to lift payloads of up to 3000 lbs. and perform complex insertion tasks that have part mating tolerances on the order of 3mm. Design of this robot is motivated by the need to reduce manpower and increase productivity by allowing one operator to perform tasks which are currently performed by a crew of up to 6 people.

This system must compensate for dynamic loads induced by shifting sea states and operate under limited visibility and difficult weather conditions. Figure 1.1 shows a concept sketch of the proposed manipulator.

The robot is a six degree of freedom serial link manipulator. In the base of the robot are yaw and pitch joints actuated by two conventional electric drive motors and gearboxes. These two axes are designated joints 1 and 2. Joint 3 is a prismatic joint actuated by a similar electric motor and gearbox. The last three joints (4-6) are roll, pitch, and yaw at the wrist of the robot. These three joints are actuated by new, high-torque direct drive electric motors. The entire manipulator is mounted on an omnidirectional vehicle which will allow it to move between payload pickup and drop-off locations.
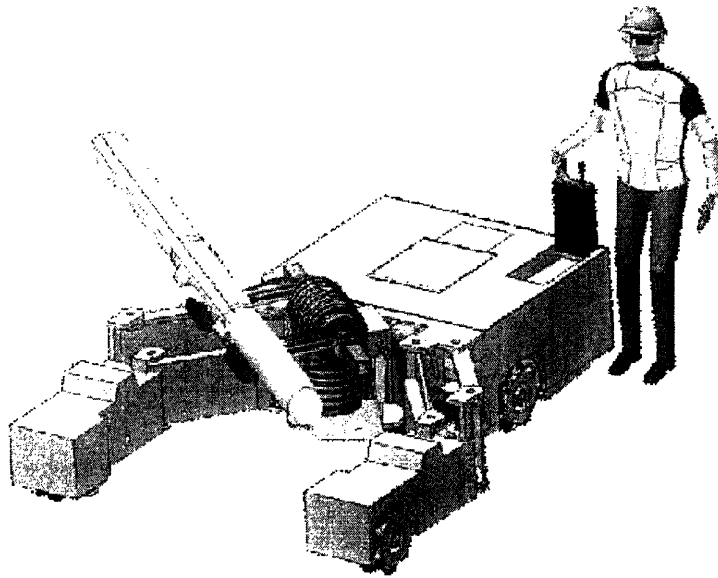
Figure 1.1: Heavy lift manipulator concept drawing

1.2 Task Description

A majority of the heavy lift tasks to be performed by this manipulator involve what are hereby defined as "simple insertion" tasks. These tasks involve very large payloads of up to 3000 lbs. These tasks involve rough positioning of attachment lugs into corresponding mating sites where they securely lock into place. These tasks have loose positioning tolerances of roughly 1cm due to friendly geometry (chamfers, fillets, etc.).

A small subset of tasks, however, requires the mating of complicated metal "hanger" structures into corresponding slots. These "complex insertion tasks" require an initial insertion followed by a sliding motion down a connecting rail enclosure. The tolerance between mating parts during the initial insertion can be as small as 2.3mm under worst conditions. The largest payload involved in this complex insertion task is only 350lbs. Pictures of these parts and a description of the motion are shown in Figure

1.2. A detailed description of the geometry required for this complex parts mating task and related tolerance calculations can be found in Appendix A.
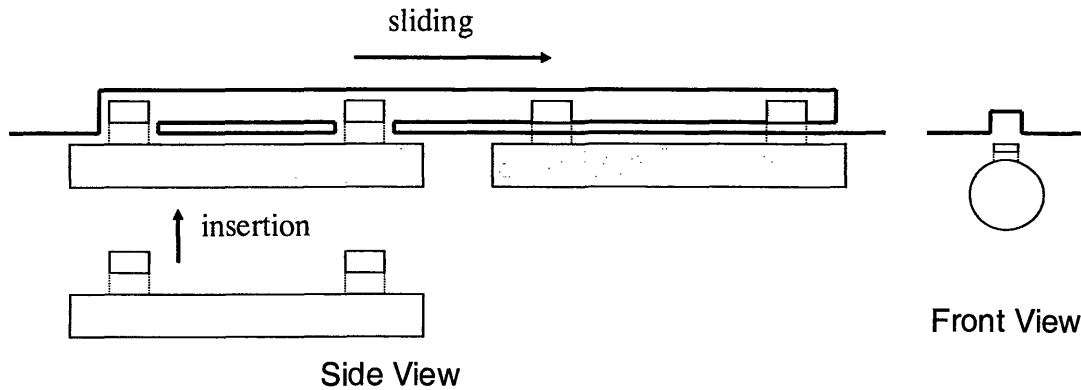
Figure 1.2: Example geometry and motion for parts mating task

1.3 Control Structure

The loose tolerances on the simple insertion tasks mean that they can be performed entirely by position commands. The operator, standing at the rear of the robot operating the joystick controls, will be able to see the task and provide the necessary position inputs to complete it. A position control system for this robot which can achieve the performance necessary for these simple insertion tasks is discussed in [15]. This controller is known as the "position controller."

Because of the tight tolerances and complex motions, complex insertion tasks require the design of an additional controller. This thesis outlines the design of this control system which is used only for these complex insertion tasks. This controller is known as the "insertion controller." During this insertion task, the operator will be at the end-effector of the robot to get the best view of the task. Commands to this controller are forces from the operator issued through the force sensing handle mounted at the end-

effector. The use of force commands instead of a joystick will give the operator a more intuitive "feel" for moving the payload, as if there was no robot and he/she was directly pushing the payload into place. The insertion controller will use the position controller as an inner structure.

1.4 Technical Problems

1.4.1 Friction

Joint friction in the robot presents a major challenge for precise manipulation. Because of the requirements to lift very large payloads, the joints in the proposed robot have large gear ratios which magnify the effect of bearing and motor friction. These friction characteristics also have load and velocity dependencies and will also change magnitude as a function of operating temperature and wear of mechanical components. To achieve the fine positioning for both the complex and simple insertion tasks it is necessary to have a controller which compensates for joint friction over this wide range of conditions.

Because contact with the environment is guaranteed during all complex insertion tasks, another significant technical hurdle in the design of the insertion control system is to overcome surface friction. This needs to be done in a robot which already has significant joint friction. The magnitude of this surface friction must be studied and, if significant, it too must be compensated in the final system.

1.4.2 Force Feedback

The insertion task is made more difficult by the inability to use bilateral force-feedback. The operator must be perform his/her control at the end-effector of the manipulator where the he/she can only observe the task visually, preventing the use of typical master/slave teleoperation systems. Telerobotic systems which have bilateral force feedback are discussed by Kazerooni [31,29] and Jacobsen [26].

In order to address the lack of bilateral force feedback, the insertion controller employs a force controller. Stability of force controllers in contact with the environment has been identified as a problem [6,22,27]. It is necessary to ensure the stability of this controller during free motions and during contact with the environment.

1.4.3 Jamming

Because the complex insertion task requires the mating of a metal part into a corresponding fixture in the environment, the interaction of these parts needs to be studied. During the insertion task it is possible for the parts to get stuck (wedged or jammed) or become damaged. The lack of bi-lateral force feedback complicates this problem by prevent the operator from having tactile knowledge of what is occurring during this interaction. There is also significant uncertainty in the friction parameters between these mating parts which must be considered.

1.5 Background and Literature Review

This thesis deals with the areas of robot force control, force control with human interaction, and robotic insertion tasks. In designing the insertion controller, lessons

learned from each of these areas have been combined to produce a system that is stable, interacts well with the user, and completes an insertion task while avoiding jamming.

1.5.1 Force Control and Human Interaction

The stability of force controllers in contact with the environment is a major problem and has been an area of fundamental research. Some key works include Kazerooni [58,27], Hogan [21], Fetherstone and Khatib [13], Newman [8] and others [7,50,56,2]. One approach to solving problem of contact stability involves carefully modeling the interaction of a robot under force control and its environment. This type of modeling has been done by Eppinger and Seering [9,10,11] and Volpe and Khosla [57,56]. These works suggest possible controller designs as well as models which can be used to study different force control strategies.

The stability problem has also been addressed through the idea of modifying impedances to produce systems which are passive to outside forces. Passive systems only dissipate energy and are found to be stable during environmental contact. Seminal works in this area include those by Hogan [18,19,20,17] and Colgate [6].

Modifying the impedance of robots has also been extended beyond the stability problem and can be implemented as a method for controlling robots. Some examples of systems which employ impedance ideas to produce systems that interact with the environment, humans, or other robots are: Newman's natural admittance control [8,39,38,16], adaptive admittance control by Seraji [48,49], object/spatial impedance control [46,12], and multiple impedance control [37]. All of these systems use a form of admittance/impedance relationship with additional work to improve performance or adapt

the framework to new tasks. This work will also use an admittance/impedance relationship with additional care taken to compensate for friction and jamming.

1.5.2 Robot Insertion Tasks

For this system, the completion of the task will also require the mating of complex mechanical assemblies. Insertion tasks have been studied widely as a classical example of robot control [33,32,1,4], specifically the peg-in hole problem [60,3,54]. Initial work on the analysis of jamming and wedging, which will be investigated in Chapter 4, can be found in Whitney [59] and Simunovic [51]. Expansion of the ideas of jamming and wedging and their application to robot control through admittance selection has been investigated by Schimmels and Peshkin [43,42,45,44] and Huang and Schimmels [23,25].

Newman [16,39] and others [36,17,5,40] have designed robots to perform similar insertion tasks, usually for the manufacturing industry. These robots each employ strategies specific to the task being performed, as is done here. Combining smaller high precision manipulators as the end-effector of larger systems is one example of this [38]. Due to the size of the payloads involved in this system, this type of hardware solution is not feasible here.

1.5.3 Similar Systems

This work can be compared to various other heavy lift systems actuated by direct human interaction. These systems are often described as "exoskeletons" because they augment human capabilities with additional strength. In this project, the robot will not be

14

worn by the operator but it is used to augment natural strength and is controlled by sensed forces from the operator. Force control for the system investigated in this thesis shares similarities with these exoskeleton systems. Fundamental work in this area can be found in Kazerooni [28, 53, 30, 29] and Jacobson [52].

A similar robot and controller has been designed by Love, Jansen, and Pin [34], which also uses the idea of augmenting human input forces through an admittance/accommodation controller. This system is used for all robot and manipulator motions, not just the final insertion task, and includes additional amplification of the user input.

This thesis combines an admittance controller similar to [34] but without the use of a human amplification gain on the user input. This system uses force control only during the insertion. The friction compensation in this controller also sets it apart. A jam prevention system is also integrated into the basic admittance control structure, unlike other robots in this area. This system comes from analysis of the part geometry, similar to [39,42,45].

1.6 Design Criteria

The fundamental design criterion for this controller is that it must allow for completion of the insertion task. Before construction of the final hardware, this criterion must be tested wholly in simulation with no human operator. One approach to overcoming this limitation is to provide the controller with a simple set of inputs. It is assumed that if the controller can operate successfully with simple inputs, the human operator will be able to do even better.

15

To prevent instability, the control system must be designed with a bandwidth one decade below the lowest structural resonance of the robot. Holding a 156kg payload, the lowest structural resonance of the robot is 9Hz. The inner-loop position controller has been designed to have a corresponding .9Hz closed loop bandwidth [15]. The bandwidth of the force controller must also adhere to this 0.9Hz limit.

To assure smooth interaction with the operator, the resultant motions of the robot must closely track the desired motions. The controller needs to settle to this desired behavior quickly so that the user "feels" the response he/she is expecting. Oscillatory responses also provide a bad "feel" to the operator and must be avoided. Because of these two considerations, the robot motion must match predicted values with a small settling time (1-2 seconds) and with minimal oscillatory behavior.

These inputs are chosen to complete the task in a predictable manner. An example input would be one that pushes the end-effector always in the direction of the target. This behavior matches what the operator would likely produce on the real system. In the field, it is expected that disturbances will occur to deviate from this simple path. With a well-trained human operator, however, it is assumed that he/she will be able to make small corrections online to ensure a completed task. With this in mind, this criterion can be stated as: the controller must be able to complete an insertion task given a set of simple user inputs.

Additionally, to allow for these small corrections which will be necessary on the real system, the controller must also be able to produce small motions when commanded. Because the parts mating tolerances are on the order of 2mm, small motions on the order of 0.5mm are the objective. It is important to note, however, that the robot will be in

contact with the environment while these small adjustment motions are made. This motion criterion must be met while in contact with the environment where surface friction is present.

1.7 System Assumptions

In addressing the insertion controller design, the following assumptions are observed:

1. The forces that the robot exerts on the environment are not felt by the user.

2. The user must act using only visual feedback.

3. The robot can (and will) limit the force signals input by the user.

4. The geometry of all mating parts is well documented.

5. Upon acquiring a payload, the robot will know the mass properties and location of the payload center of mass.

6. A "wrist force sensor" is used to measure all forces applied directly to the payload. These include contact forces, inertial disturbance forces, and environmental disturbances (wind, etc.). See Figure 1.3.

7. A "user input sensor" measures the user's force command inputs and it is assumed that this sensor is not subject to external disturbances. See Figure 1.3

8. All contact forces and input forces are transformed into the end-effector coordinate frame.
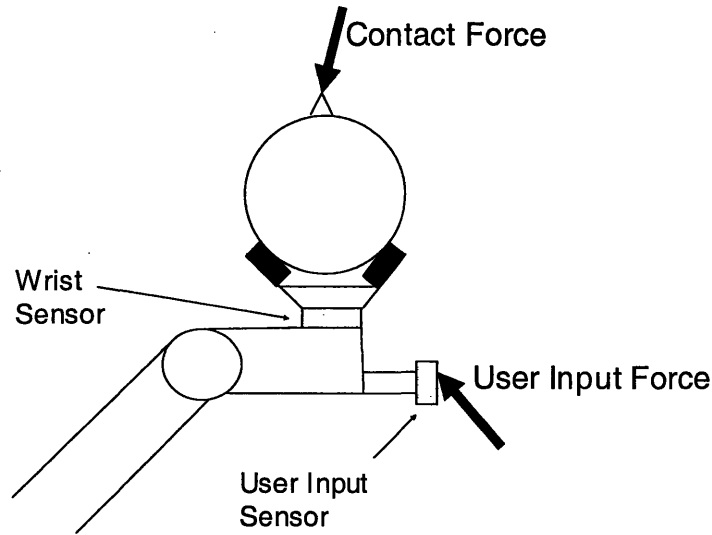
Figure 1.3: Proposed sensor placement at manipulator end-effector

1.8 Control System Architecture

The chosen insertion controller is an admittance based force controller with the position controller designed by Garretson as an inner loop [15]. An admittance controller generates velocity commands from force signals (either force inputs from the user or force feedback from the environment). An additional inner-loop positioning system is required to move the robot to this desired velocity. For the insertion controller, this inner loop is a joint space PID controller with joint friction, gravity, and ship motion compensators. There are six individual PID controllers whose gains are all chosen to achieve a closed loop bandwidth one decade below the lowest structural resonance of the system [15]. Because the payload mass has a major effect on system structural resonance, gain scheduling based on payload is used.

Gravity compensation is performed through a kinematic calculation of joint torques required to hold the robot steady at a given position in the presence of gravity.

18

As mentioned earlier, friction compensation is a major technical challenge facing the insertion controller. Sensor based torque feedback loops are used on the first three joints of the robot. Due to hardware limitations, however, sensor based feedback is not possible on the last three joints. Here, an adaptive algorithm is used to calculate friction compensation torques [14]. This adaptive system also provides estimates of parameters that can be used to estimate models of joint friction [15].

During the insertion task, contact forces are likely to invalidate the adaptation laws, rendering it dangerous. Therefore, the information from this scheme is used to generate friction parameter estimates. During the insertion task, a friction model is used to compensate for friction on these last three joints. As the robot positions the payload close to the insertion points, estimates for the friction models are updated and used by the feed forward compensator. Because of this constant updating, these estimates account for changes in the robot hardware due to normal wear and tear or temperature changes. During insertion control, the adaptive estimator is turned off and the friction parameter estimates are held at their pre-contact values.

The detailed position controller, with the friction and gravity compensation schemes, in shown in Figure 1.4.
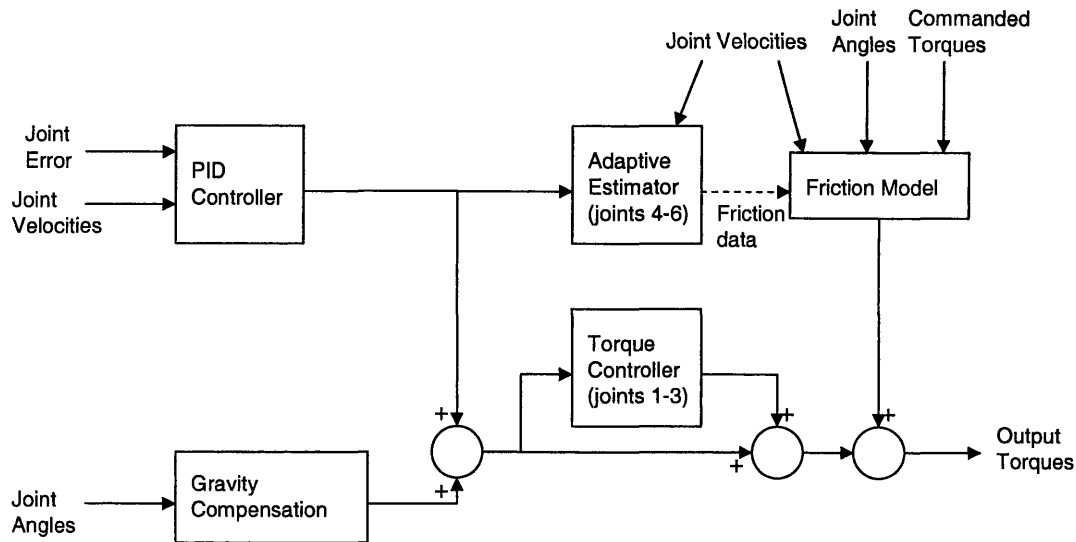
Figure 1.4: Implementation of position controller subsystem

The admittance controller works by taking forces from either the user or the environment and transforming them into desired velocities through a transfer function called the admittance law. Choosing different structures for this transfer function generate different motions. Typical admittance laws are limited to mass/spring/damper behaviors. The Cartesian velocity generated by the admittance law is transformed into joint velocities by means of the inverse Jacobian matrix and integrated to produce desired joint positions. The position controller then exerts the required joint torques to move the robot as desired.

In this system, the gravity and friction compensators in the position controller can be thought of as system for negating gravity and friction, thus "floating" the payload and robot. The admittance law, in conjunction with the PID controllers, creates the motion corresponding to the user's input forces.

By using contact forces as a feedback signal, this admittance controller also controls contact forces to desirable levels. The block diagram for this admittance controller with user inputs and contact force feedback is shown in Figure 1.5.
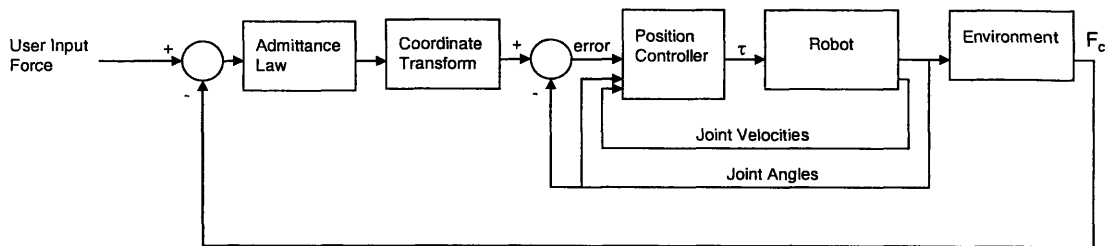
Figure 1.5: Basic structure for insertion controller

1.9 Thesis Outline

This thesis presents details of the design of the insertion control system, shows simulation results validating its capabilities, and analyzes the jamming problem and presents a possible scheme for online jam avoidance.

Chapter 2 describes the details of force and interaction control strategies. A procedure for analyzing the stability of the chosen force controller, using an established environment model, is also presented. This procedure will be employed to derive stable admittance law gains when the final hardware is constructed and experiments can be performed to determine values for the relevant parameters of the models presented.

Chapter 3 contains simulation results showing how the performance of this controller meets the design criteria set forth in this chapter. Chapter 4 addresses the

21

problem of part jamming after the initial mating portion of the insertion task is completed. Also in this chapter, the use of jamming models to design a jam prevention controller is presented. Finally, conclusions for future work and possible verification studies are discussed in Chapter 5.

ADMITTANCE CONTROLLER DESIGN

2.1 Overview of Possible Strategies

The core function of the manipulator is to assist the user in lifting a heavy payload while moving it to align lugs on the payload into corresponding support fixtures. Most of the torques exerted by the robot control system are used to support the load [28,55]. A combination of only a gravity compensator and friction compensator is shown in Figure 2.1. This system, which has no position set-point, simply "floats" the payload, supporting the load for the operator. External forces, either from a human or the environment (such as contact forces) will act on the combined inertia of the robot and
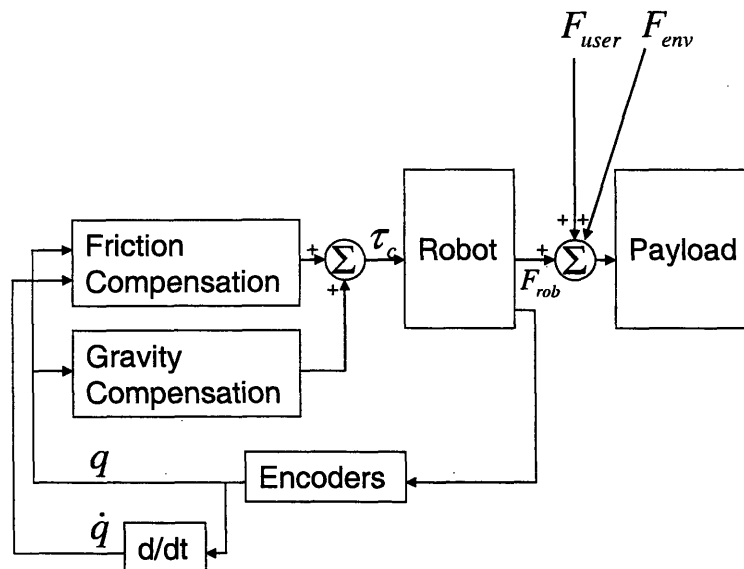
Figure 2.1: Floating payload setup: gravity and friction compensation only

payload to cause motion.

This basic system represents an effective tool for manipulating large payloads. Manipulation can be performed by directly applying forces to the payload. For small payloads these interaction forces would be small, making it easy to manipulate. For large payloads this system may require too much effort from the operator. This system does not provide any ability to modify the inertia of the payload felt by the operator.

Systems have been proposed that can modify the effective inertia of robot, such as Hogan's impedance control [18,19,20]. This method prescribes a desired Cartesian impedance behavior to a robot and applies the appropriate control torques to make the robot respond as if it had this desired impedance. It is called impedance control because, as formulated, the input is an imposed position/velocity. The controller takes this position/velocity information and calculates the required torque to apply to the robot joints.

This control scheme is ideally suited for robots which have very low natural impedance (low joint inertia and back-drivability in all joints). In these types of robots, the user can prescribe arbitrary positions and velocities to the robot. The controller then generates torques based on the error between its desired position and the position imposed by the operator.

In this system, there is a large natural impedance due to large joint masses, large payload, and high gear ratios. This makes it unsuitable for an impedance control approach. Instead, the concept of impedances is inverted to create an admittance controller. In an admittance controller, the input is a force (instead of a position) and the

output is a position/velocity command (instead of a force). By reacting to input forces, this system implements the same payload interaction of the purely gravity/friction compensated robot mentioned above while still allowing for modification of this interaction. Details of this scheme are discussed next.

2.2 Admittance Control

An admittance controller translates input forces into desired velocities. With a desired velocity provided, an additional control element is used to exert the necessary servo action to move the robot to this desired velocity. This can be done either with a velocity feedback loop or by integrating the desired velocity and using it as the input to a position feedback loop. In this system a position feedback approach is used. The position controller used is the one already designed for moving the robot prior to the insertion task (see [15] for details of this controller). This allows for a smooth transition between position and insertion control by simply changing the input source from the joysticks to the force sensor handle under the payload.

Sciavicco and Siciliano have suggested that using a velocity based controller provides better force following than a position based controller [47]. Use of an velocity based controller may be an avenue to pursue in future work but is not explored here.

Figure 2.2 outlines the strategy of adding an admittance controller on the user input to the gravity/friction compensation framework. The position controller is added to exert the necessary control torques required to implement the given admittance law. The

implementation of the position controller (here called a joint controller) is the same as discussed in Chapter 1.
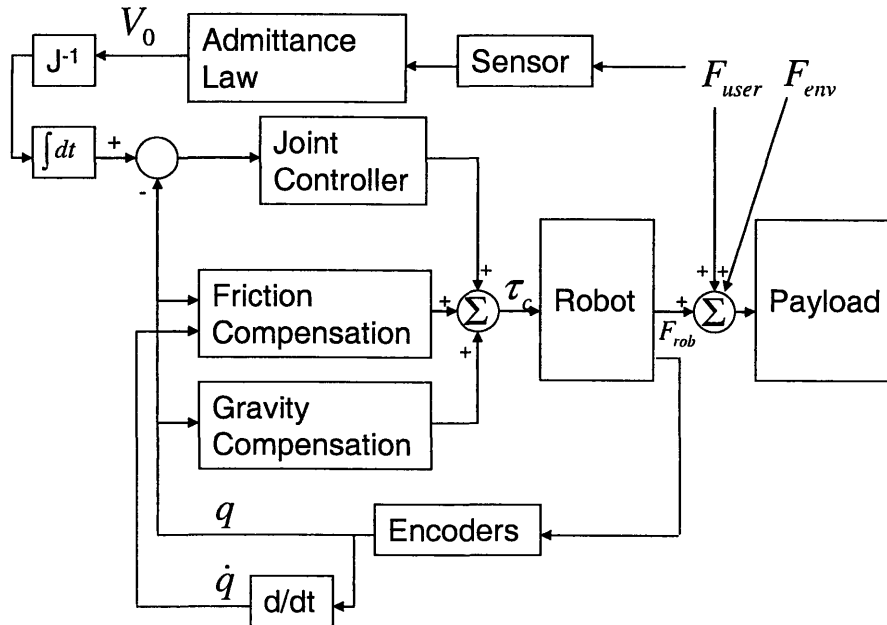
Figure 2.2: Admittance controller implemented on user input forces

2.3 Insertion Controller

To this point, the discussion of the control system has focused on the user input forces, applied via application through a sensor and admittance law as defined above. It is also necessary to compensate for environmental contact forces. The admittance controller setup can be used again to compensate for contact forces, as measured by the wrist sensor (for sensor locations see Figure 1.3). The resulting control system setup is shown in Figure 2.3.

The following assumptions are made in this implementation of the admittance controller:

1. F_{ref} is set to a full vector of zeros, meaning that the controller will act to control all contact forces and torques to zero.

2.   The wrist sensor measures all forces applied to the payload. This signal does not include user input forces.

3.   The same admittance law is applied to user input forces and contact forces.

By applying these assumptions to the system shown in Figure 2.3, the resulting force controller looks exactly like the one shown in Figure 1.4. The user input force sensor provides a reference signal and the force measured by the wrist sensor becomes the force feedback signal.
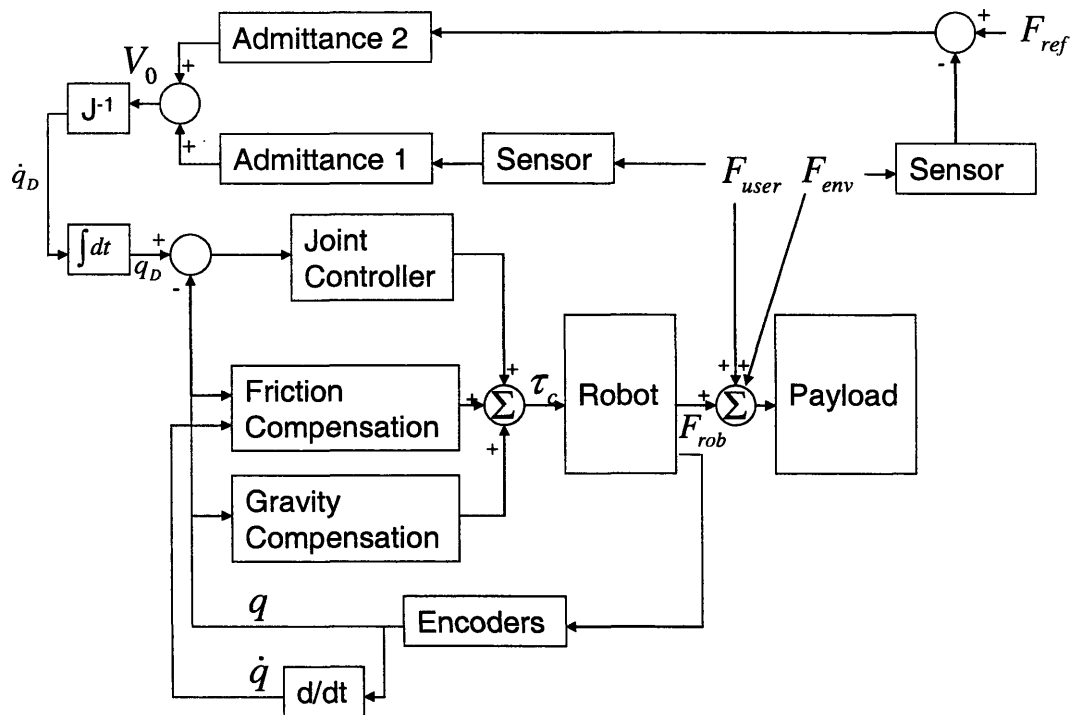
Figure 2.3: Full admittance controller setup including sensors on both user and environment forces

2.4 Environment Interaction Analysis

Now that an appropriate controller has been chosen, it is necessary to determine controller gains that achieve desired performance and stability and meet the design constraints. The major constraint for this system is a bandwidth limitation. The structural resonance of this system when holding a 350lb. payload is 9Hz. To account for this, the position control system was designed to have a closed loop bandwidth 1 decade below, or .9Hz. Gains for the admittance law are also chosen so that the closed loop bandwidth of the insertion controller remains at .9Hz.

Figure 2.4 shows a one degree of freedom plant model for analyzing robot force controllers initially proposed by Eppinger and Seering [9,10,11] and later employed by Volpe and Khosla [57,56]. It uses inertias as the major dynamic component and includes spring/damper elements to represent their interaction. The two blocks (M_R and M_S) represent the mass of the robot and sensor respectively. On the robot side is a spring damper (K_R and B_R) representing the robot's stiffness and damping. Between the two masses is a spring damper pair representing the sensor (K_S and B_S). Beyond the sensor mass, the last spring damper pair models the environment (K_E and B_E).

Input: Controller Force – F

Output 1: Robot Position – X_R

Output 2: Contact Force – $K_S(X_S-X_R)$
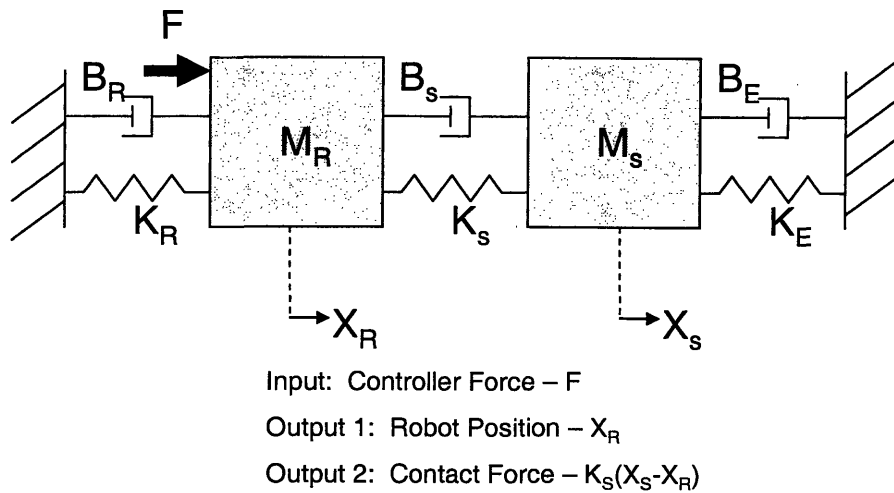
Figure 2.4: Fourth order environment interaction model for robot force controllers

The papers by Volpe and Khosla use experimentally derived parameters in this model. Analysis of numerous controllers showed that pure integral control provided the best resulting force tracking and stability. However, a second order low-pass filter also showed promising performance. This is promising, because a purely damping field admittance law would result in an integral controller and the addition of an inertia to this admittance would add a second order behavior. An admittance law consisting of damping and inertia is therefore a sensible choice and should provide good performance and stability. Details of these admittance laws are discussed later.

However, two additional changes need to be included in this environment model to capture the dynamics of the insertion task. The first change is to include a large payload mass located beyond the wrist force sensor. The second change is to add a compliance between the wrist sensor and the payload to represent compliance in the robot's gripper. Modifications of this type are discussed in Eppinger and Seering [11].

29

Incorporating these additional elements into the model shown in Figure 2.4 creates the final model shown in Figure 2.5. The additional mass (M_P) represents the mass of the payload and the additional spring/damper pair (K_G and B_G) models the compliance in the robot's gripper.

Input: Controller Force – F

Output 1: Robot Position – X_R

Output 2: Contact Force – $K_S(X_S-X_R)$
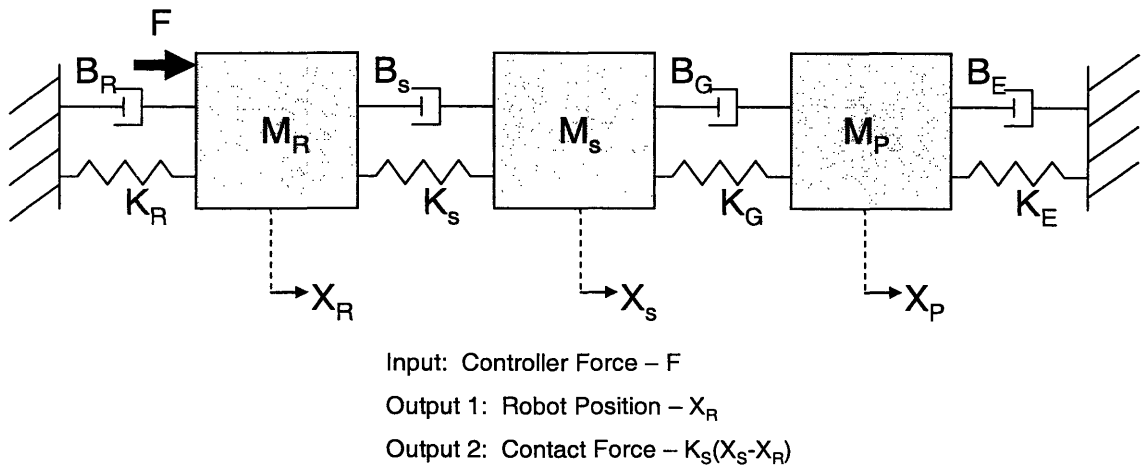
Figure 2.5: Interaction model modified to include gripper compliance and payload

The dynamics of this system are strongly tied to the parameters chosen for the various elements of the model. To observe what effect these changes have on the choice of controller architecture, this plant can be matched with various controllers. The performance of the controller and plant can then be observed.

The approach for selecting the final admittance law is to combine this plant model with a model of an admittance controller and investigate the closed loop stability using classical control techniques. The complete derivation of the equation for the plant and its integration with a PID/Admittance controller is shown in Appendix B.

2.5 Admittance Law Selection

The procedure for selecting an appropriate admittance law first consists of choosing a desired behavior. With this behavior chosen, the transfer function of the insertion controller and plant can be calculated. By observing the closed loop bandwidth of this system, appropriate gains for the admittance law are chosen to achieve desired performance and bandwidth.

For a single degree of freedom system the framework of possible admittance laws is described by the transfer function:

$$G(s) = K_S \cdot s + K_D + \frac{K_I}{s} \tag{2.1}$$

Here, G(s) defines a transfer function from an input force to an output velocity and K_S defines a spring constant, K_D defines a damping coefficient, and K_I defines an inertia.

Design of the insertion controller focuses on two admittance types: purely damping (K_S=0, K_I=0) and damping plus inertia (K_S=0). Spring behavior (nonzero K_S) is ignored because it has the effect of adding a position dependency. This position dependence is an anchor point for a virtual spring that is attached to the end-effector of the robot. If not specified, the position of the robot when the insertion controller is activated would become this set-point and the spring behavior would act to drive the robot back to its starting point. This is undesirable for the insertion task. Also, differentiating a force signal is problematic because force sensor readings are generally noisy.

Once the robot is constructed, it will be necessary to perform tests similar to those outlined by Volpe and Khosla [57] to determine the spring, damping and mass parameters of the environment models discussed above.

2.6 Chosen Admittance Law

Using estimated values of the model parameters, two different admittance laws were found which both adhere to the required bandwidths: a damping law of $K_D=1.75 \times 10^{-5}$ and a mass-damper with $K_I=2 \times 10^{-5}$ and $K_D=1.5 \times 10^{-5}$. Force following plots for these admittance laws are shown in Figure 2.6. The dotted lines represent the commanded force and the solid lines represent the resulting contact force. An overdamped response is clearly visible in the pure damping case. The addition of an inertia term in the second plot shows additional overshoot but no oscillatory behavior. The relevant parameters used in this analysis, including the gains for the position control inner loop, are included in the derivation in Appendix B. Because of its better performance, the purely viscous admittance law is implemented in the insertion controller.

This admittance law results in a motion of about 0.8mm/s with an input force of 45N (10lbs.). This is acceptable because a highly damped admittance provides slow, well controlled motions. The time scale of 15-20 seconds for this task and the length scales of 5-10cm of motion are achievable with this admittance law without excessive effort from the user. These results meet the design criteria for performance while maintaining an overall closed loop bandwidth of .9Hz.
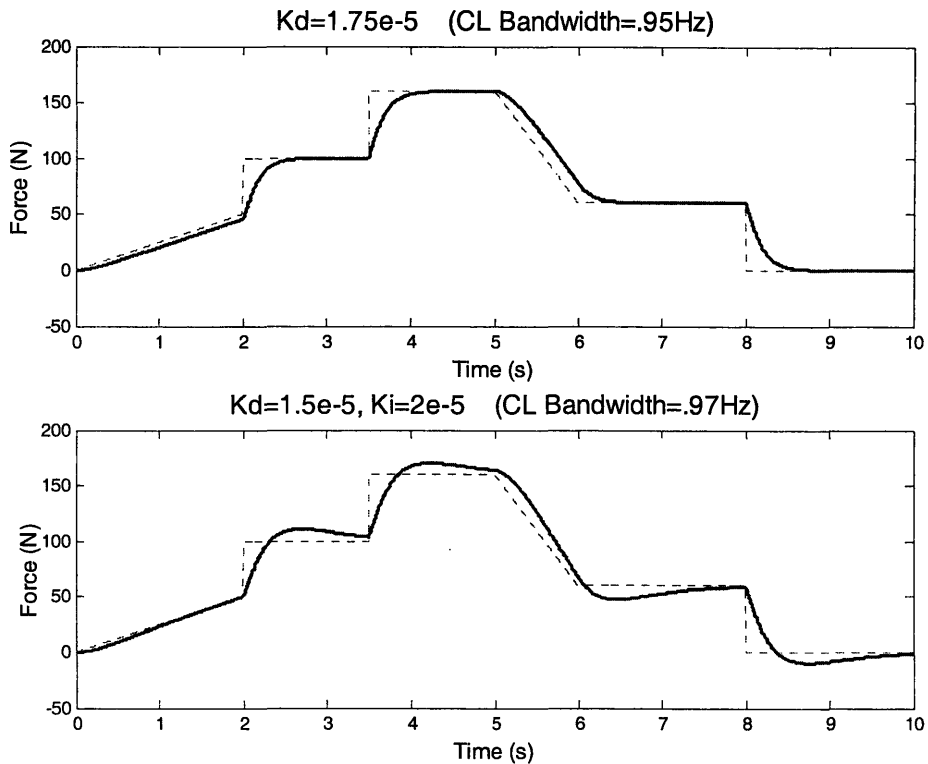
Figure 2.6: Example force following for two chosen admittance laws

Extending this simple admittance law to the full controller, which has six forces and torques, requires a 6x6 matrix. In this matrix, each diagonal element corresponds to the admittance for one Cartesian direction (x, y, z, roll, pitch, yaw). This equates to a matrix of transfer functions. In the case of the purely damping admittance law used here, the full admittance law matrix is a constant diagonal 6x6 matrix of K_D gains.

Peshkin and Schimmels [42] have written extensively on selecting nondiagonal admittance laws which are proven to provide desirable reaction forces to all possible contact forces (to prevent jamming, for instance). Although the controller presented does not require a diagonal admittance matrix, the presence of nondiagonal terms would create non-intuitive force reactions to the user. A linear force input could result in a rotational motion of the end-effector. For this reason, all admittance matrices in this system are

kept diagonal. Jam prevention is achieved through a different system which is discussed in Chapter 4.

For the rest of this thesis, the admittance law used is a diagonal matrix of $K_D=1.75 \times 10^{-5}$. After the robot is constructed, these gains can be tuned further using the environment interaction model updated with empirical data. The exact structure and values of the admittance law need to be chosen with an operator experimenting on the real system. This will allow for an admittance law that provides an intuitive feel to the operator.

SIMULATION RESULTS

3.1 Simulation Goals

The goal of computer simulation is to verify that the proposed insertion controller can meet the overall design objectives established in Chapter 1:

1. The controller must be able to successfully insert the part given a simple, ideal set of user inputs. This is tested by simulating the robot, payload hangers, and mating sites in the environment. This setup uses a simulated human operator giving force commands based on visual feedback.

2. The user must be able to make small adjustments to the payload position while in contact with the environment. This will allow the user to manually compensate for disturbances. This criterion is tested by applying small user force inputs and observing the resulting motion.

For these studies, the controller is tested with both ideal and worst case conditions for joint friction compensation. The ideal case establishes a benchmark for the best possible performance. The worst case uses poor joint friction compensation that eliminate only 80% of the actual joint friction in the system.

3.2 Friction Compensation

3.2.1 Joint Friction

In all of these simulations, the major factor affecting the success of the insertion task is the friction compensation. To revisit the assumptions about friction compensation:

1. During the insertion task, the robot is in contact with the environment and contact disturbances disrupt the adaptive friction compensators. These compensators must be turned off.

2. The position controlled tasks, which occur before the insertion task, require large motions of all manipulator joints and provide sufficient excitation to identify friction parameters.

3. Model based open loop friction compensation will be used during the actual insertion task in place of the adaptive compensator.

Discrepancies may exist between the actual friction in the robot and the models used in the feed-forward compensator, especially in the area of nonlinearities around zero velocity which can result in a stick-slip behavior. Sensitivity studies to gauge the affect of these discrepancies will be discussed in Chapter 5.

3.2.2 Surface Friction

Surface friction during the insertion task represents a disturbance that is difficult to model. Tests with the actual hardware show the static Coulomb friction coefficient to be

0.31 and the dynamic Coulomb friction coefficient to be 0.26. Analysis shows that surface friction is significantly smaller than joint friction. Table 3.1 shows an RMS average of the joint friction on all six robot joints, taken from a simple motion simulation. For a standard 100N contact force (Y direction), the generated surface friction of 31N is projected to the joints via the transpose Jacobian matrix in both the X and Z directions. The resulting disturbance torques are on the order of 1-2% of the total joint friction, with the exception of joint 5 where it is about 50%. Joint 5, however, has friction levels an order of magnitude less than all other joints. The magnitude of this disturbance is the same as or smaller than the expected errors in the joint friction compensator. For this reason, surface friction does not require a separate compensator.

Joint Number	RMS Average Friction	Surface Friction (X)		Surface Friction (Y)	
		Value	Percent	Value	Percent
1	5486.7 (Nm)	55.13	1.00%	-9.68	0.18%
2	1070.1 (Nm)	1.04	0.10%	-11.27	1.05%
3	4059.3 (N)	-3.31	0.08%	30.16	0.74%
4	617.8 (Nm)	1.07	0.17%	-10.12	1.64%
5	28.1 (Nm)	0.00	0.00%	-15.69	55.85%
6	254 (Nm)	0.00	0.00%	0.00	0.00%

Table 3.1: Comparison of joint friction and surface friction magnitudes.

3.3 Simulation Environment

All simulations are performed with Adams 12.0 to calculate the forward dynamics of the robot with Simulink block diagrams for all control system elements. Adams calculates the resulting robot motion from the input torques calculated from the controller

in Simulink. To do this, Adams needs the physical properties of the robot: link dimensions, kinematic configuration, and link inertias. All joint friction is handled through Simulink as a disturbance; however the surface friction and contact forces are more complex and are modeled along with the robot in Adams.

3.4 Insertion Task Simulation

The simulated insertion is designed to analyze the controller's ability to complete the insertion task with an intelligent set of user inputs. In this simulation, the human inputs come from a simple visual feedback system. The simulated user sees the displacement of the payload away from its target and applies the necessary force to move it into place. The focus of this simulation is on successful completion of the task with simple imputs, as defined by the design criteria.

Figure 3.1 illustrates the robot's initial pose and coordinate frame for these simulations.
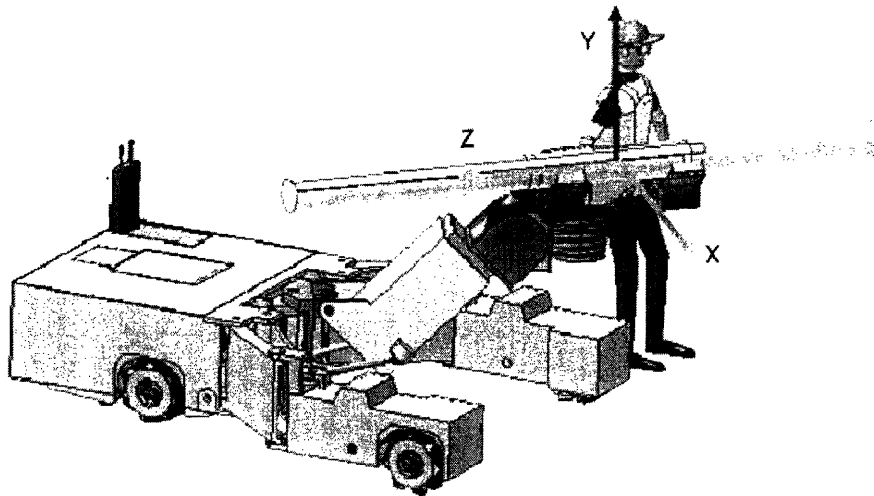
Figure 3.1: Manipulator configuration and coordinate frame for insertion simulation

3.4.1 Setup and Inputs

The model used in these simulations is a complete representation of the manipulator shown in Figure 1.1. The position controller is the same one described and designed in [15]. The friction compensator on the last three joints turned off and replaced by a model based feed-forward system.

This simulation uses an operator model based on visual feedback as the input. A measure of displacement between the end-effector and the target is calculated to represent the user observing the task. This displacement is used as the input to a PD controller to generate force outputs to feed into the admittance controller. The forces determined by the PD controller are upper bounded at 225N (50lbs) to prevent excessive strain on the user and lower bounded at 12.5N (3lbs) to ensure that the motion does not stall when the

error signal gets small. The input signal also includes a positive offset in the upward direction to produce a steady contact force with the environment of 110N (25lbs.).

3.4.2 Results

The simulated user is able to complete the task in the ideal, no joint friction case. The controller tracks the input forces well and produces a smooth motion of the robot. The effect of surface friction is minimal. Figure 3.2 shows the error in the X direction as the payload approaches the insertion point. Two vertical lines indicate the times at which the first and second lugs engage with their mating slots. The 2mm positioning tolerance in the X direction is indicated by the horizontal dotted line. Because this is a measures of the displacement of the center of the payload and the lugs are located on the ends, one of the lugs engages before the tolerance is met. This is understandable because the payload has a yaw error. While the payload is tilted, one lug is closer to its target and the other further away. Figure 3.3 shows the contact forces maintained during this task. The level of the vertical (Y) force can clearly be seen to track the desired 110N. The sharp drops in this force correspond to the first lug engaging at 23 seconds and the second lug engaging at 32 seconds.
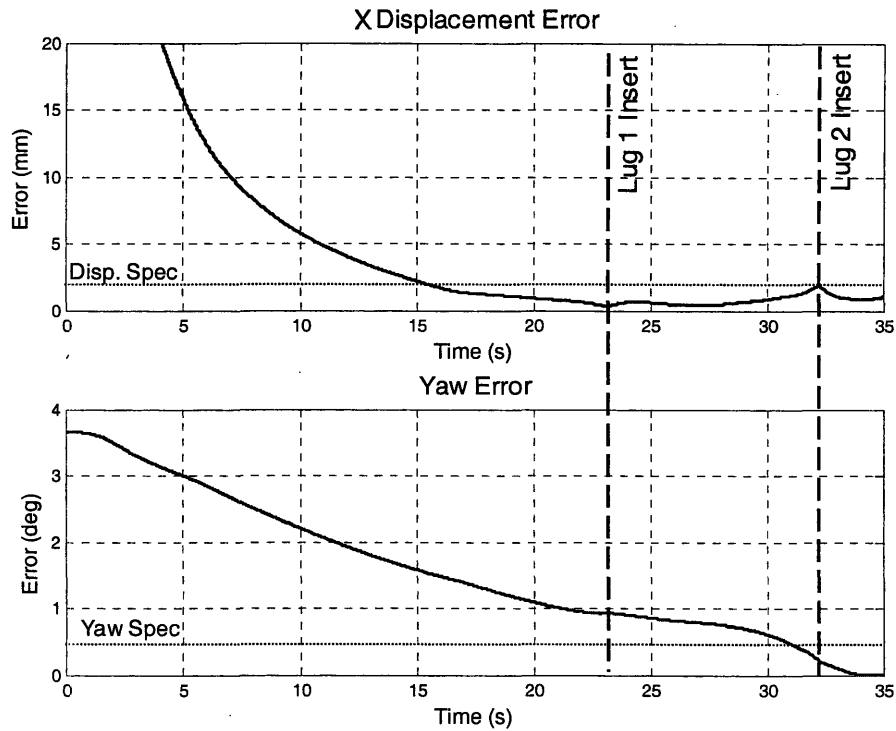
Figure 3.2 Tracking error during insertion simulation, no friction

Even in the worst case of 20% uncompensated joint friction, the simulated user is again able to complete the task, satisfying the design constraint. Figure 3.4 shows the same tracking error plot for this case. The jerky motion of the robot can be attributed to the uncompensated joint friction. Figure 3.5 shows the contact forces measured during the task. In this case, the controller stays within a band that is +/-10N from the desired level. This deviation can again be attributed to the significant joint friction. Again the positioning tolerance is represented by the horizontal dotted line.
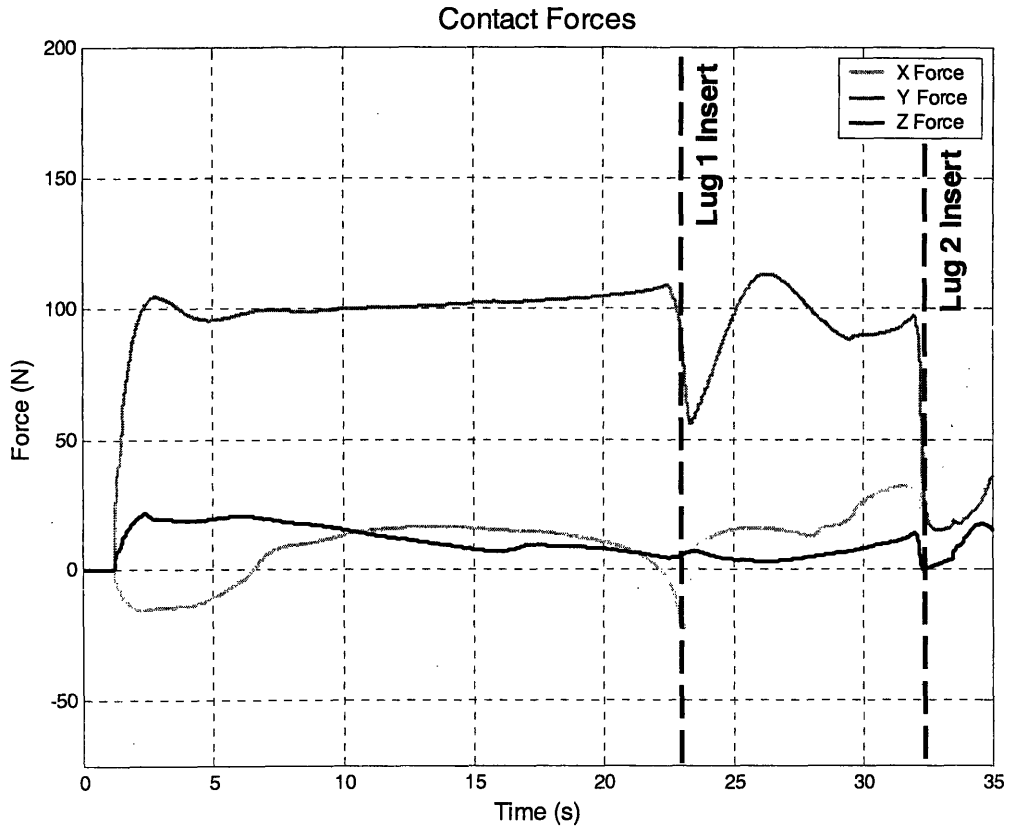
Figure 3.3 Contact forces during insertion simulation, no friction

X Displacement Error

Figure 3.4 Tracking error during insertion simulation, 20% uncompensated friction

Contact Forces

Figure 3.5 Contact forces during insertion simulation, 20% uncompensated friction

43

3.5 Resolution Studies

Two tests were performed to observe the control system's reactions to small adjustment forces. In both tests the robot is commanded to move into contact with the e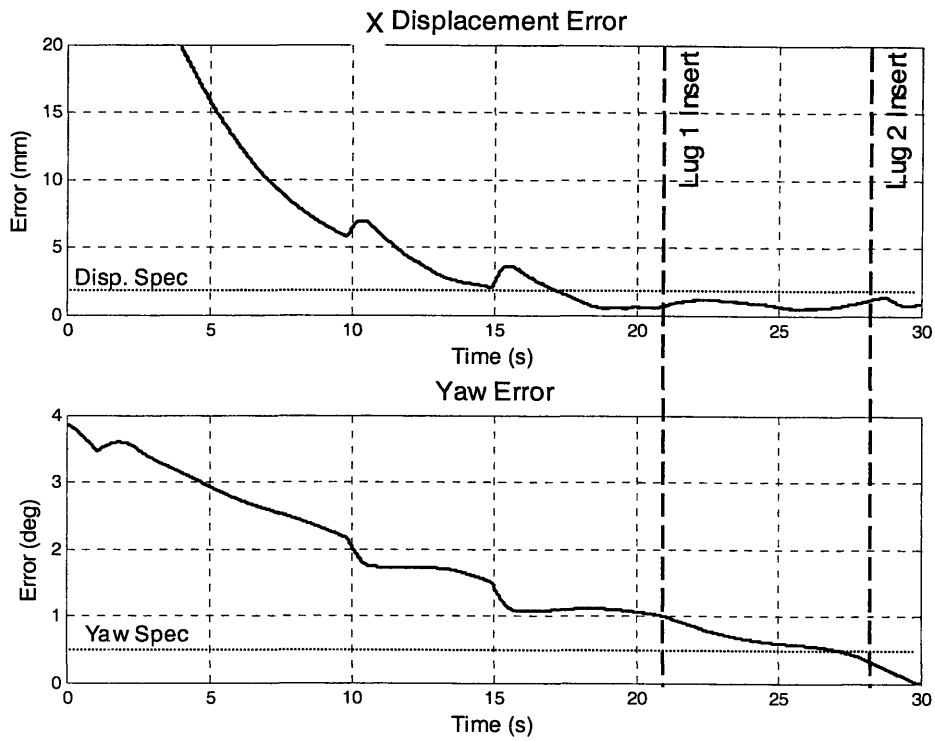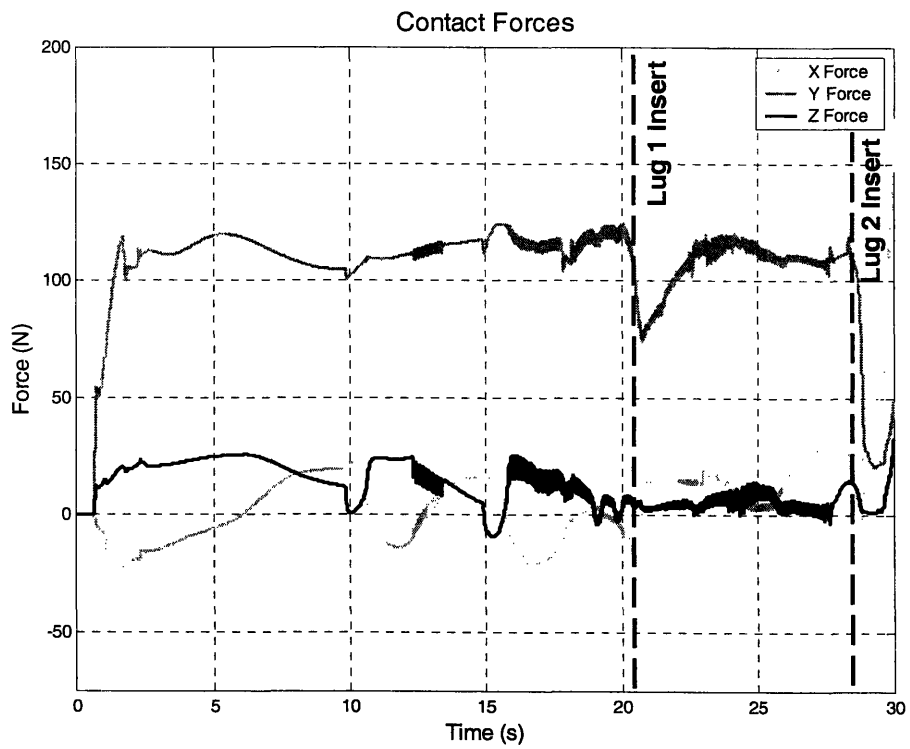nvironment and maintain a constant upward (Y direction) force of 100N. All forces which generate motion are performed after transients in this vertical force have died out.

The first test uses three square wave signals of varying intensity to move the payload. These three input waves have magnitudes of 25N, 50N, and 75N, and each has a duration of 1 second. With the 100N contact force, the surface friction resisting motion should have a value of 31N. Because of this, it is expected that the first input of 25N will result in no motion of the payload.

Figure 3.6 illustrates the resulting contact forces during this test. The dotted lines represent the desired forces and the solid lines the actual measured forces. This graph shows two things. First, the ability for the admittance controller to maintain forces levels with the environment is shown by observing the contact force in the Y direction. Secondly, the effect of surface friction in the feedback path is clearly shown. With the 25N nudge, the friction reaction force rises to the level of the input and no motion results. In the 50N and 75N nudges, the friction level rises only to the level of the dynamic friction. The difference between the input signal and the reaction force, coming from friction, produces the motion.
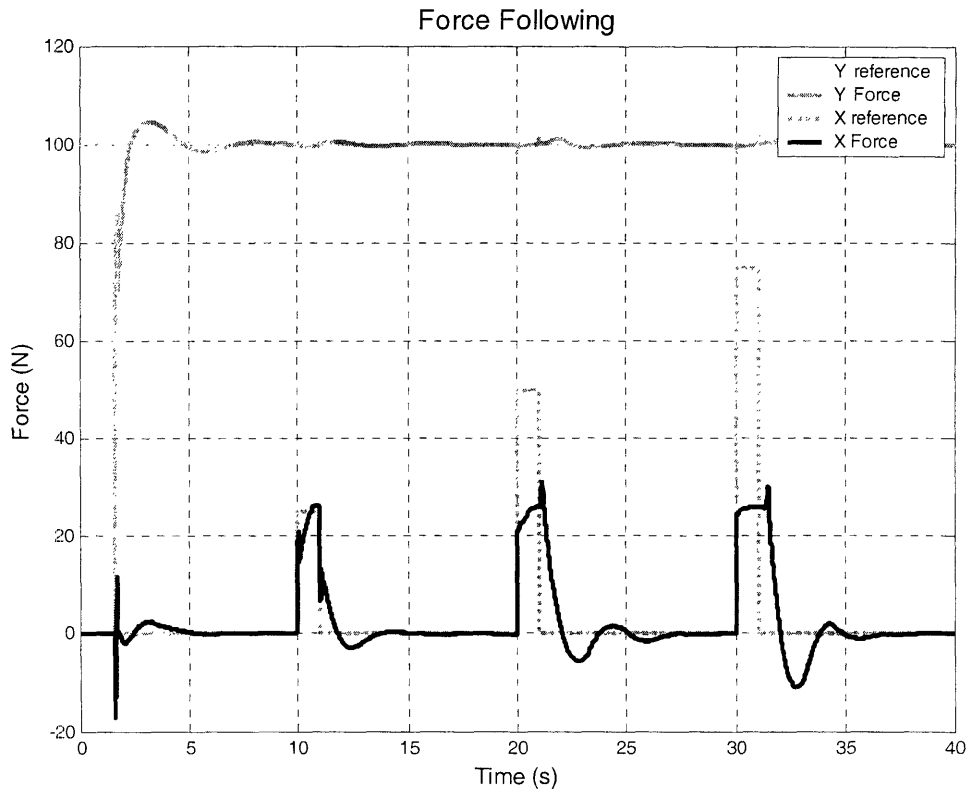
Figure 3.6 Force following for three square wave force inputs

Figure 3.7 illustrates the resulting motion of the robot. As expected, the robot does not move with the first nudge. The second and third nudges produce motions of 1.3mm and 3.5mm.

Resulting Robot Motion
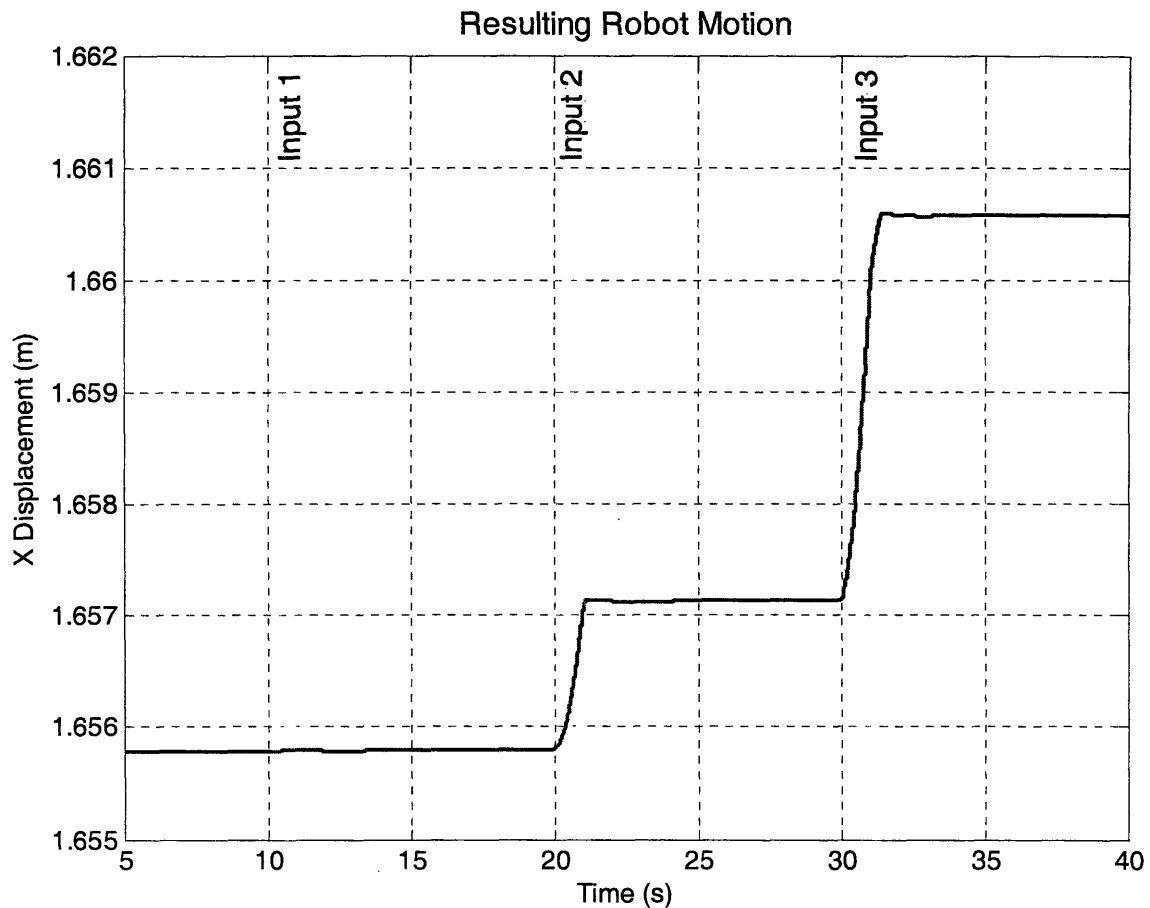
Figure 3.7: Resulting motion from three square wave force inputs

The second test uses one input which simulates a user just barely trying to break free of the surface friction. The desired behavior is for the user to slowly ramp up the input force until the payload breaks free of surface friction and starts to move. Once motion is detected, the user stops pushing.

The input signal starts at 0N and ramps slowly up to 31N, at which point it is expected that the payload will break free of surface friction. At this point the user should see motion occurring. A 0.5 second delay is included after the force reaches 31N to incorporate human reaction time. After this reaction time, the input force is halted. Figure 3.8 illustrates this user input.

Figure 3.9 illustrates the resulting motion for this input for the ideal case and for the worst case 20% uncompensated joint friction. The ideal case produces a motion of 0.6mm, very close to the design specification of 0.5mm. The case with joint friction, however, actually produces a smaller motion of 0.3mm. This is likely due to the robot joint friction adding natural damping. Once the payload breaks free of the surface friction, the robot will move slower in the presence of joint friction.

The resulting small motion is close to the range of 0.5mm specified in the design criteria and is considered acceptable. The presence of uncompensated joint friction needs to be tested further. In the case of a low estimate, smaller motions like those seen in Figure 3.9 can be expected from the increased damping. If the friction estimates used in the feed-forward model are larger than the real values, the magnitude of this small motion could increase.
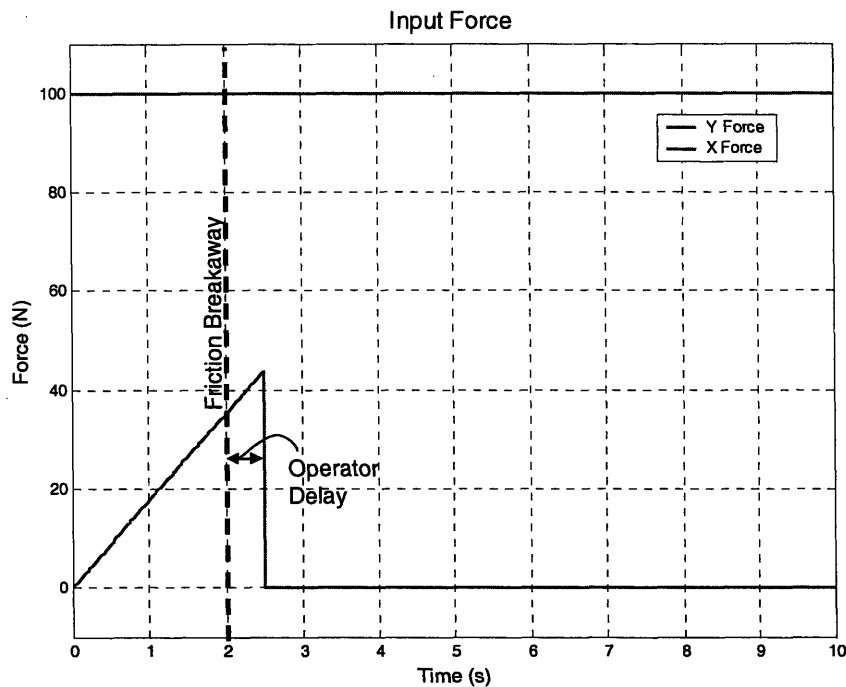

Figure 3.8: Force input profile for small motion test.

Resulting Robot Motion

No Joint Friction

20% Joint Friction

X Displacement (mm)

Time (s)
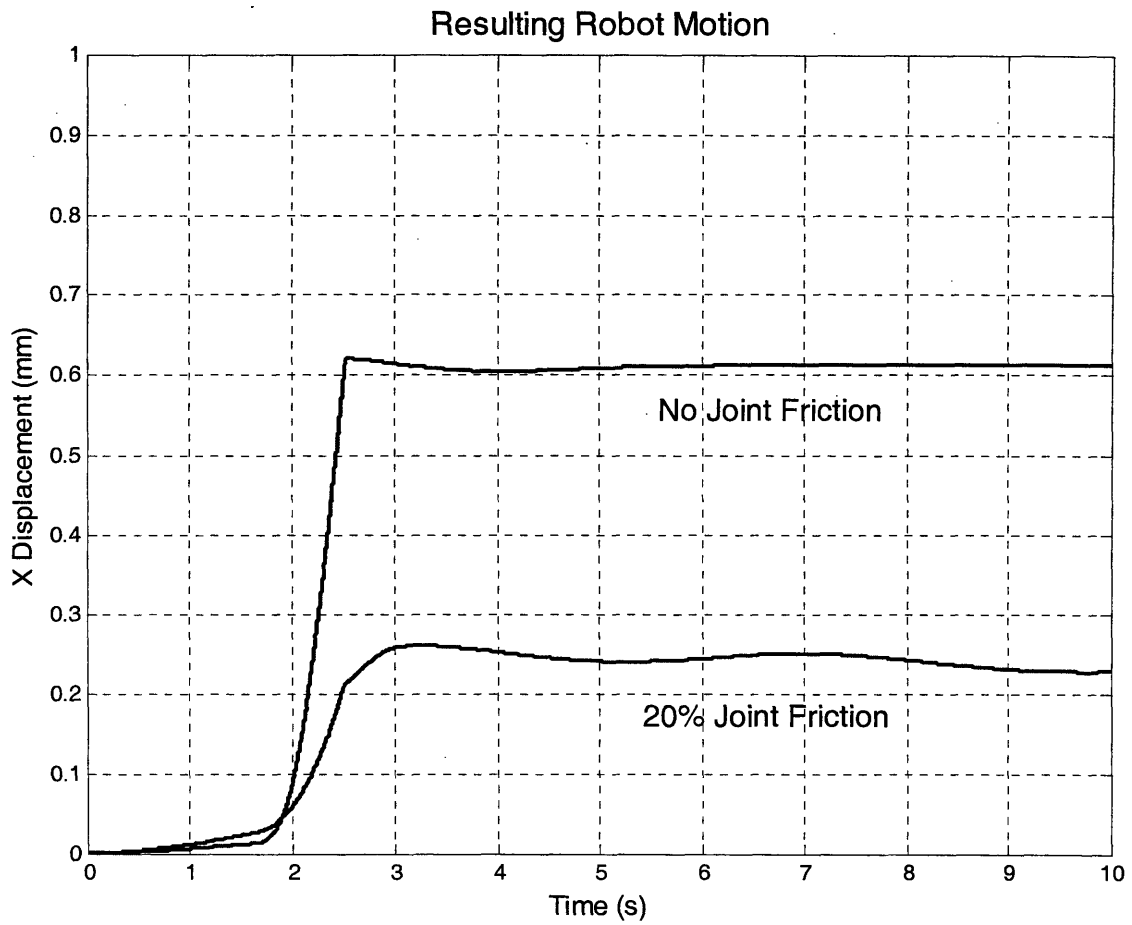
Figure 3.9: Resulting motion for small input test, no friction and 20% friction cases

CHAPTER

4

JAMMING ANALYSIS AND PREVENTION

4.1 Motivation

The peg-in-hole problem is well studied as a benchmark for robot manipulation and force control [60,3,54]. Two distinct challenges of these tasks include wedging and jamming, as defined by Simunovic [51] and referenced in Whitney [59].

Wedging is defined as a state in which the inserted part contacts the mating surface and becomes statically held in place by the contact forces alone. This occurs when the friction cones from each contact point overlap. See Figure 4.1 for an illustration. A familiar example of wedging is a drawer getting stuck at a sharp angle when pulled out too far. This type of wedging only occurs at the very beginning of an insertion task when the contact points are close to each other. When this occurs it becomes completely immobile to both pushing and pulling. Because of this, wedging is an unrecoverable state. Removing all forces which cased the wedge will not cause the part to become "unstuck."

Jamming, on the other hand, is defined as a state in which the contact forces applied to the object provide sufficient frictional force to overcome the forces attempting to push the part down a corresponding slot. This state involves no overlap of friction

49
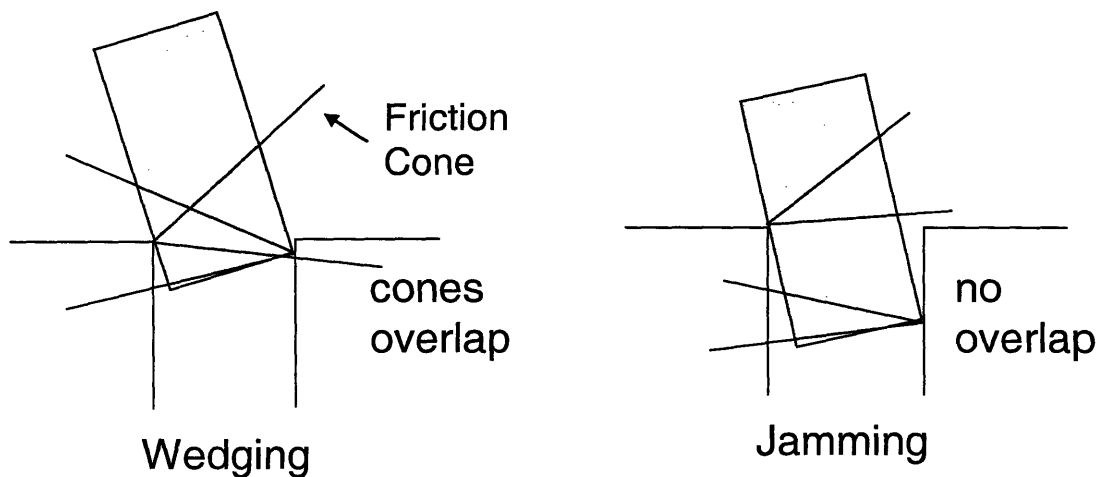
Figure 4.1: Comparison of wedging and jamming for planar peg-in-hole insertions

cones at any of the contact points and, because of this, generally occurs when the part has move significantly down its slot.

Jamming is a recoverable problem. Removing all applied forces will reduce the friction until the part can move freely. Alternatively, the input force can also be increased to a level which will overcome the jamming friction.

There is no danger of wedging given the geometry of the parts in the complex insertion task, but there is a high risk of jamming. The required motion is illustrated in Figure 4.2, it consists of two distinct motions: an initial insertion followed by a sliding motion down a long slot. It is during this sliding motion the risk of jamming is high. For this analysis, it is assumed that the user has operated the manipulator to achieve the initial mating. The jamming analysis during this chapter will assume the robot is traveling down the slot.
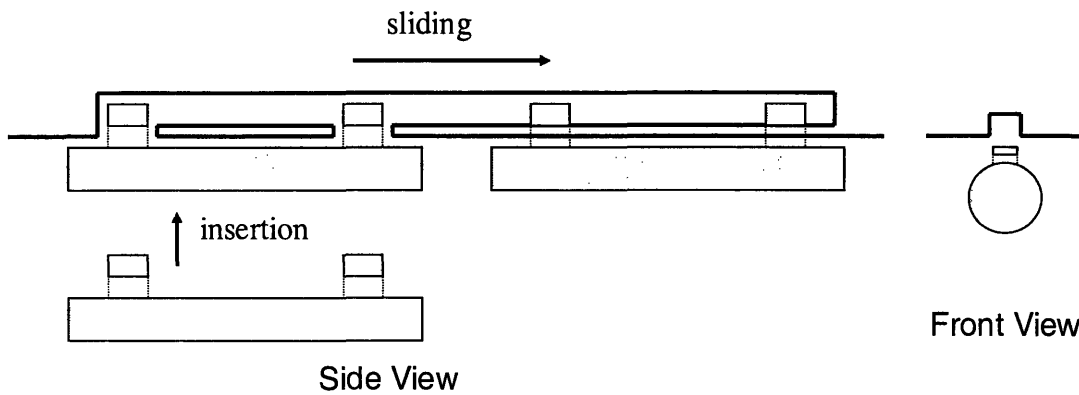
Figure 4.2: Required motions for complex insertion task

Without bilateral force feedback it is possible that the user will not be able to feel the difference between a jamming state and a free motion state. The motion required for the robot to move the part from a free state to a jammed state is on the order of millimeters. This small motion is difficult to detect even in ideal situations; in field conditions it will be very difficult. A system that monitors the user input and prevents jamming would be useful. Figure 4.3 shows such a jam prevention element placed in the insertion control block diagram.

The final design of this prevention system is outlined below. It makes use of knowledge of the geometry of the sliding parts and calculates a corrective force ΔF required to prevent a jam from occurring. The final output of this system is the corrected user input $F+\Delta F$, as shown in the Figure 4.3.
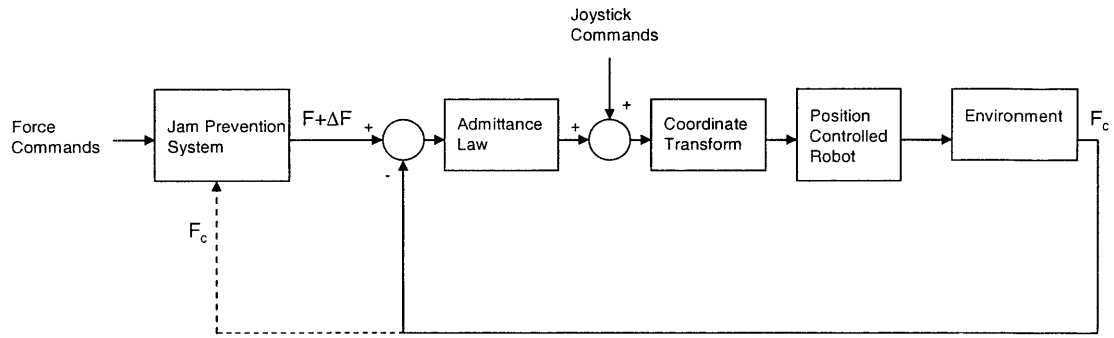
Figure 4.3: Insertion controller with jam prevention system

4.2 Derivation of Jam Conditions

In this section a set of equations which determine the ways in which the rectangular

part can become jammed is calculated. Jamming is defined as a state in which the total

friction exerted on the part is greater than the force pushing it down the slot. A set of

inequalities therefore results from this analysis which provides limits on the input forces.

To illustrate the geometry more clearly, refer to Figure 4.4, which gives dimensions and

relevant directions for this sort of slot motion task. It is assumed that the length Lx is

significantly larger than both Ly and Lz and that all rotational displacements within the

slot are small. The parameters used to express the jamming conditions are the force

pushing the part down the slot: Fx, and all forces/moments which affect the contact

forces: Fy, Fz, Mx, My, Mz.
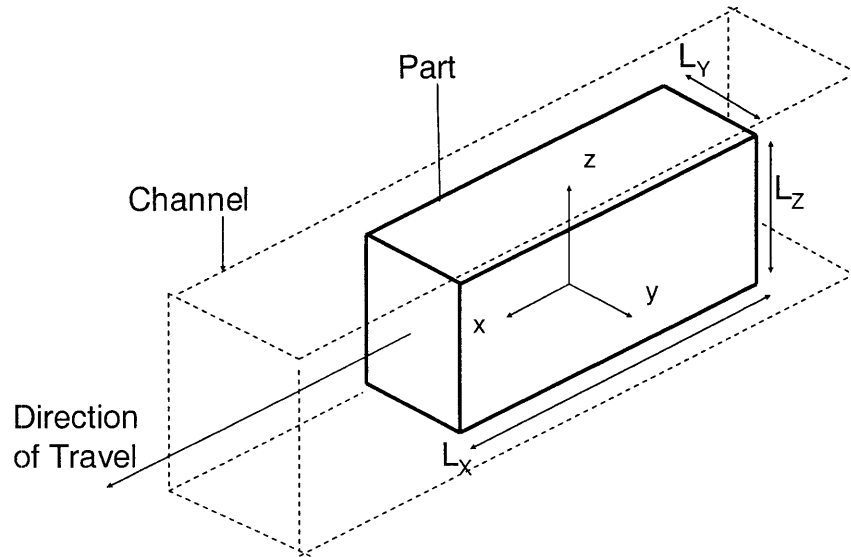
Figure 4.4: geometry and coordinate frame for part insertion task discussion

The basic inequality condition states that a jam will occur if the total frictional force, F_f, which is a function of the five applied forces and moments, is greater than the force down the slot, F_X:

$$F_f > F_X \qquad (4.1)$$

The friction force, F_f, is solely in the X direction and it is calculated based on the set of inputs: Fy, Fz, Mx, My, Mz. These inputs can affect the total friction in two ways: through forces and moments. For the two linear forces, the equation for friction is:

$$F_f = \mu \cdot F_N \qquad (4.2)$$

where μ is the coefficient of friction and F_N is the relevant normal force (either the Y or Z direction). For angular moments, the friction equation is similar, but includes the relevant length term:

$$F_f = \frac{\mu \cdot M_N}{L_N} \qquad (4.3)$$

For Y and Z rotations, the length is L_X. For rotations about X, there are a few possibilities. In this system, the geometry is such that the slot is wider in one dimension and rotations about the X axis will only result in two point contacts. L_y is the relevant length dimension for these contacts.

It is now necessary to calculate how the friction forces from the various inputs can combine in to create the total friction felt by the part. Some spatial reasoning over possible stable configurations of a square peg in a square channel result is required. One possible spatial configuration is outlined in Figure 4.5.
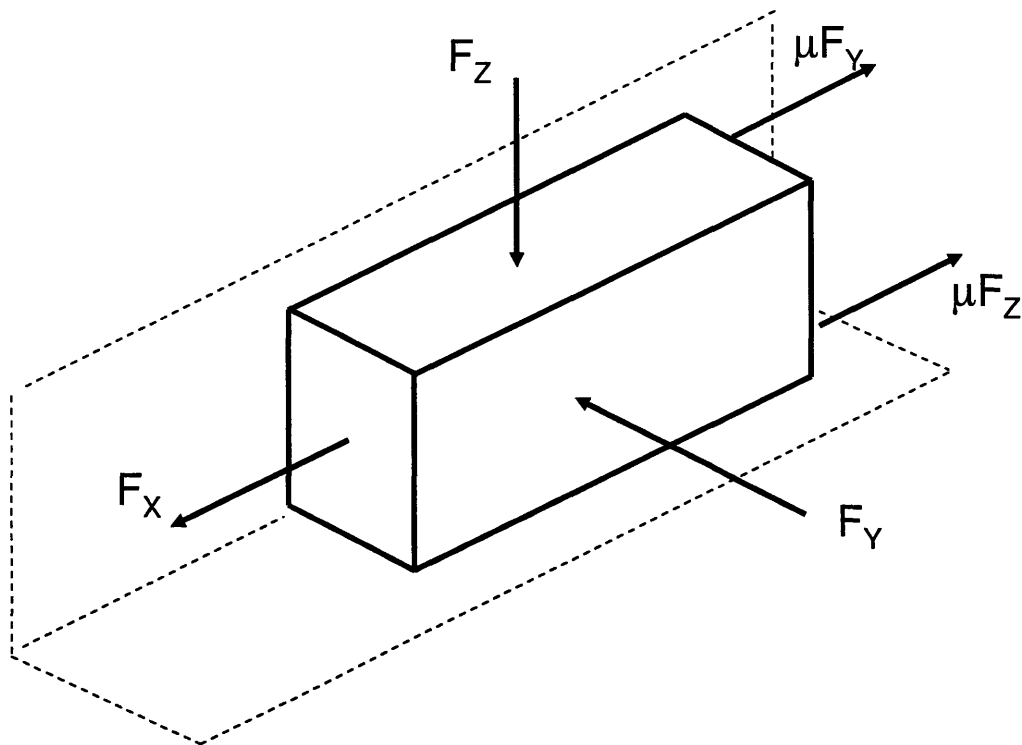
Figure 4.5: Free body diagram of one possible jamming state

This configuration is defined as "flat-flat" as it involves flat contact on two faces. As the free body diagram shows, each of the two friction terms is calculated from the related normal force. The total friction force must be larger in than F_X for the part to be jammed. This is illustrated in Equation 4.4:

$$F_f = \mu \cdot F_Y + \mu \cdot F_Z \qquad (4.4)$$

Combining equations 4.4 with 4.1 and dividing by F_X to normalize the inequality results in the following:

$$\frac{\mu \cdot F_Y}{F_X} + \frac{\mu \cdot F_Z}{F_X} > 1 \qquad (4.5)$$

The force down the channel, F_X, was moved to the left side of this equation for simplicity and to make the resulting condition unity. If this condition is true, the part is considered jammed.

There are four other jamming conditions which are illustrated in Figure 4.6. Each of these four has a friction equation similar to 4.4 with the relevant input forces and lengths. The normalized inequalities for all five of these jamming states is the following:

$$\text{Flat - Flat:} \quad \frac{\mu \cdot F_Y}{F_X} + \frac{\mu \cdot F_Z}{F_X} > 1$$

$$\text{Flat - Twist:} \quad \frac{\mu \cdot F_Z}{F_X} + \frac{\mu \cdot M_Z}{L_X \cdot F_X} > 1$$

$$\text{Twist - Flat:} \quad \frac{\mu \cdot F_Y}{F_X} + \frac{\mu \cdot M_Y}{L_X \cdot F_X} > 1 \qquad (4.6)$$

$$\text{Twist - Twist:} \quad \frac{\mu \cdot M_Y}{L_X \cdot F_X} + \frac{\mu \cdot M_Z}{L_X \cdot F_X} > 1$$

$$\text{X - Tilt:} \quad \frac{\mu \cdot M_X}{L_Y \cdot F_X} > 1$$

55

Flat-Flat   Flat-Twist   X-Twist

Twist-Flat   Twist-Twist
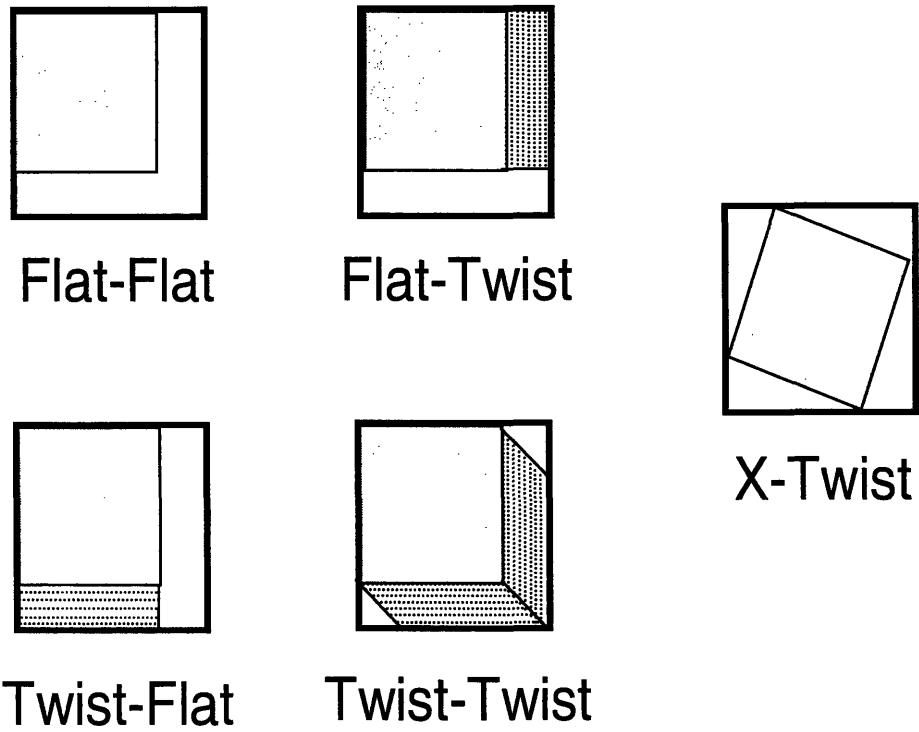
Figure 4.6: Five possible jamming configurations for rectangular part

These five conditions can also be written in a matrix equation as:

$$
\begin{bmatrix}
\dfrac{\mu}{F_X} & \dfrac{\mu}{F_X} & 0 & 0 & 0 \\[2ex]
0 & \dfrac{\mu}{F_X} & 0 & 0 & \dfrac{\mu}{L_X \cdot F_X} \\[2ex]
\dfrac{\mu}{F_X} & 0 & 0 & \dfrac{\mu}{L_X \cdot F_X} & 0 \\[2ex]
0 & 0 & 0 & \dfrac{\mu}{L_X \cdot F_X} & \dfrac{\mu}{L_X \cdot F_X} \\[2ex]
0 & 0 & \dfrac{\mu}{L_Y \cdot F_X} & 0 & 0
\end{bmatrix}
\cdot
\begin{bmatrix}
F_Y \\ F_Z \\ M_X \\ M_Y \\ M_Z
\end{bmatrix}
>
\begin{bmatrix}
1 \\ 1 \\ 1 \\ 1 \\ 1
\end{bmatrix}
\qquad (4.7)
$$

The 5x5 matrix on the left is based only on the force down the channel (F_X), the geometry, and the friction coefficient. It is called the jamming matrix, J. The five forces which affect the friction levels are placed in a vector F_C. The product of J and F_C calculates all five jamming criteria and are placed in a vector, γ:

$$\gamma = J \cdot F_C \tag{4.8}$$

This new vector, γ, contains all the information about jamming. The jam conditions can now be expressed as:

$$|\gamma|_\infty > 1 \tag{4.9}$$

All elements of this vector are unit-less and a value of 1.0 in any element will mean a jam is occurring.

4.3 Jam Prevention System

4.3.1 Constraint Analysis

The jamming conditions derived above, expressed in the J matrix, can be viewed as constraints on the values of F_C. There are five total constraints spanning the five dimensional space of the F_C vector. These two dimensions do not need to be the same. In different geometries there could be additional constraints, in which case the J matrix will have more than five rows.

For clarity, a two dimensional version of this constraint problem is shown in Figure 4.7. In this figure, F_C is a 2-d point on the plane and there are three constraints: γ_1, γ_2 and γ_3. Each of the constraints is a row from the J matrix and each forms a linear

boundary in the F_C plane. In the example shown, γ_3 represents the boundary that is closest to the contact force, F_C.
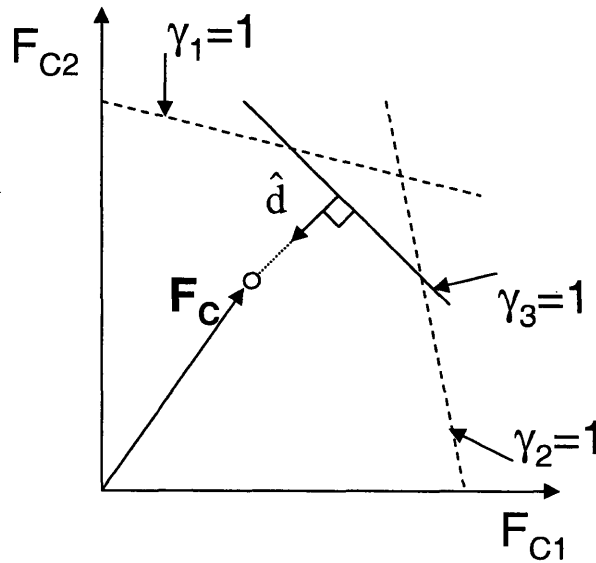
Figure 4.7: Two dimensional example of force monitoring with three jamming boundaries

With jamming defined as boundaries on F_C, it is possible to derive a system to determine the optimal adjustment to F_C which will act to move it away from the closest boundary. The closest boundary represents the jam condition that is most likely to occur. As mentioned above, γ_3 is the closest boundary to the current F_C position in this example. Because it is desirable to move the F_C location away from this boundary, it is necessary to know the normal vector perpendicular to it. This vector is labeled in Figure 4.7 as d.

4.3.2 Force Correction

With this information about constraints, it is possible to generate a force correction signal. Once the γ vector is calculated, the largest element of this vector represents the closest boundary and the most likely jamming state. The best correction

signal is one that will move F_C away from this boundary and reduce the likelihood of the corresponding jam condition from occurring.

If the location of this element in the vector γ is N, to calculate the proper displacement vector, d, the Nth elements of Equation 4.8 provides all the relevant information. It can be rewritten as:

$$[\gamma]_N = [J]_N \cdot F_C \tag{4.10}$$

In this equation, the row vector $[J]_N$ represents the normal of the γ_N boundary, which contains the same direction information as the vector labeled d. The direction of d points optimally away from the Nth boundary. To adjust F_C to move away from this boundary with a ΔF "push", the direction is now known, but the magnitude not.

To reduce the jamming risk, it is necessary to choose a sensible magnitude for ΔF based on γ. A linear scaling of γ by a gain K would achieve this desired effect and could be written explicitly as:

$$\Delta F = -K \cdot \gamma \cdot \left(\frac{[J]_N^T}{\left\| [J]_N \right\|} \right) \tag{4.11}$$

With K•γ as vector length for the correcting force, the resulting force will grow as the boundary is approached and continues to grow (without bound) once it is crossed. This is a desirable behavior, but this K gain does not need to be constant. Figure 4.8 illustrates other examples of possible methods of calculating the magnitude of this correcting factor.
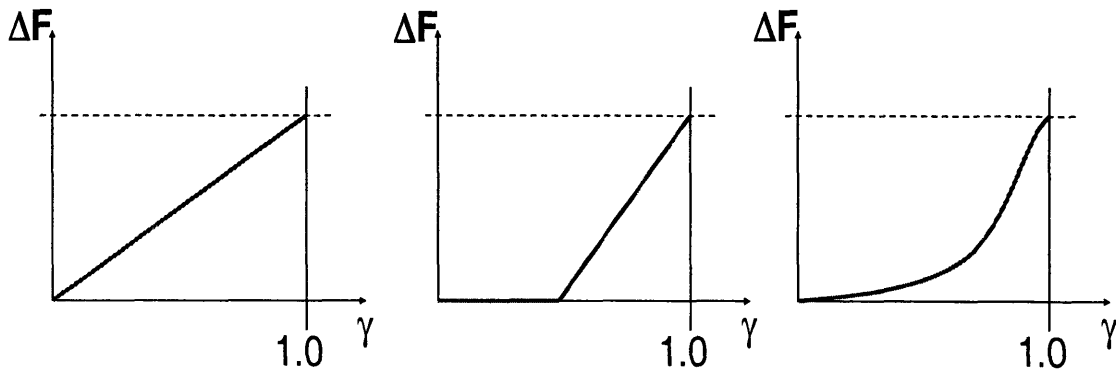
Figure 4.8: Examples of functions used to calculate the length of ΔF vector

The first function shown is the same linear gain just discussed, but the other two represent solutions which would have little or no effect when the F_C location is safely near zero but exert increased effort, possibly in a linear or quadratic manner, as the γ signal starts approaches 1. The threshold used in the second example function or the exact shape of the nonlinear function shown in the third example function could be determined by experimentation. As long as the function resides wholly in the first quadrant it will achieve the desired result of driving F_C away from a jamming state.

Because the F_C vector, and the corresponding ΔF which is calculated to correct it, do not include the F_X vector (the force acting in the direction of travel) this system will

never generate the trivial solution of "increase F_X" in order to overcome friction. This is very desirable in a system with a powerful manipulator and fragile parts which could break under excessive force. The ΔF corrections here always act to reduce the normal forces as the method to reduce and overcome friction.

It is now possible to outline the procedure for the jam prevention block as described in Figure 4.3:

1. Calculate the appropriate jam condition matrix, J, based on the commanded F_X signal.

2. Calculate γ by multiplying J with F_C.

3. Find the location of the largest element of the γ vector, N.

4. Isolate the Nth row of the J matrix.

5. Using the isolated row vector, calculate the correction factor ΔF based on Equation 4.11 using an appropriate (and possibly nonlinear) K gain.

6. Output the initial user command with the ΔF correction added.

4.4 Principle Jam Conditions

In the case of the geometry presented in this thesis, determining the 5 possible jamming states can be accomplished simply by observation. However, in more complex systems this may not be possible. An alternative solution is to calculate the effect of each input by itself, ignoring the possible ways that they can combine. This involves applying the input forces one at a time and deriving the corresponding jamming equations. This

61

procedure will always result in the same number of jamming conditions as the number of inputs. The resulting jamming condition equation for this situation is:

$$
\begin{bmatrix}
\dfrac{\mu}{F_X} & 0 & 0 & 0 & 0 \\[2ex]
0 & \dfrac{\mu}{F_X} & 0 & 0 & 0 \\[2ex]
0 & 0 & \dfrac{\mu}{L_Y \cdot F_X} & 0 & 0 \\[2ex]
0 & 0 & 0 & \dfrac{\mu}{L_X \cdot F_X} & 0 \\[2ex]
0 & 0 & 0 & 0 & \dfrac{\mu}{L_X \cdot F_X}
\end{bmatrix}
\cdot
\begin{bmatrix}
F_Y \\ F_Z \\ M_X \\ M_Y \\ M_Z
\end{bmatrix}
>
\begin{bmatrix}
1 \\ 1 \\ 1 \\ 1 \\ 1
\end{bmatrix}
\qquad (4.12)
$$

This matrix of jamming conditions will be called P, for principle jam conditions, and it is acted on by the same input force vector, F_C. The jamming conditions can be rewritten as:

$$
P \cdot F_C = v
$$
$$
|v|_\infty > 1
$$
$$
(4.13)
$$

The v vector resulting from this analysis will be a sufficient but not necessary condition on jamming. A value of 1.0 in v will indicate a jamming state, but there will be conditions where all values are less than 1.0 but can combine in such a way to produce a jam. An example of this would be values of 0.75 in the first two elements of this v vector. This would correspond to Y and Z forces that are each 75% of the required jamming force. Analyzing this situation with Equation 4.4 shows that the friction from both the Y and Z faces will add linearly and produce $\gamma_1 = 1.5$, indicating a jam.

It is also possible to calculate a relationship between the J and P matrices definted as:

62

$$J = S \cdot P \qquad (4.14)$$

Here, S is a selection matrix which adds the various principle components in the proper manner to produce the J matrix. For this case, the 5 possible jamming states result in the following S matrix:

$$S = \begin{bmatrix} 1 & 1 & 0 & 0 & 0 \\ 0 & 1 & 0 & 0 & 1 \\ 1 & 0 & 0 & 1 & 0 \\ 0 & 0 & 0 & 1 & 1 \\ 0 & 0 & 1 & 0 & 0 \end{bmatrix} \qquad (4.15)$$

On other systems, the S and J matrices may be difficult to calculate. The number of rows these two matrices correspond to the number of possible jamming configurations and may be very large for complex systems. The number of inputs, however, remains constant and could be calculated experimentally by measuring the resulting motion of test inputs that isolate the various elements of F_C.

Although it does not capture all possible jamming states this system does still create boundaries in the F_C space and can be used in the jam prevention system in the same manner with the following modification to Equation 4.11:

$$\Delta F = -K \cdot v \cdot \left(\frac{[P]_N^T}{\|[P]_N\|} \right) \qquad (4.16)$$

The effectiveness of 4.16 over 4.11 remains to be measured through experiment and is a suggested avenue for future research.

CHAPTER

5

CONCLUSIONS

5.1 Experimental Verification

The models used in Chapter 2 to choose proper admittance law gains need to be based on experimentally measured parameters. Some of these parameters (compliances, for instance) can be measured directly while others (damping coefficients) require indirect methods such as measuring the response to test inputs. With experimental parameters in the environment interaction models, a more accurate choice of admittance law can be made. Final tuning of this admittance law with the help of the constructed robot is needed to determine a control response that has the right "feel" to the user.

5.2 User Interface Studies

The presence of a human simplifies many of the control problems if he/she is expected to make intelligent decisions about inputs to the system. For example, errors in gravity compensation will make the robot sag below the desired target. With this error, a human operator can simply provide a small upward compensating adjustment. This is an example of the human correcting for the robot, but additionally the robot can provide some corrections to the human. Many mistakes that the human could make with a force input would have a large amount of high frequency information: hand jitters or sharp

impulses. The insertion controller discussed here can be used to filter or reduce these undesirable effects.

Experiments to verify these interactions of the human and robot can be performed independent of robot hardware and task geometry and would provide a great deal of insight into controller design for this category of manipulators.

5.3 Sensor Accuracy

Because it is used as the feedback signal during the insertion task, the reading from the wrist force sensor is critically important. As such, sensor fidelity needs to be addressed. Drift in this sensor could direct the robot in the wrong direction. Additionally, if there is a large discrepancy between the wrist sensor and the user input sensor, improper velocity signals could result. A logical next step for this research would be to conduct a thorough study of system sensitivity to errors in the force signal.

5.4 Suggestions for Future Work

This thesis is divided into two main branches of work so there are logically two additional avenues for future work. The first portion, chapters 2 and 3, deals with designing an interaction system for a robot controlled by an operator applying forces directly to the end-effector. There are numerous experiments which can be performed on laboratory hardware to determine ideal choices of admittance laws. An interesting avenue of research may be to determine a system of choosing admittance laws without the presence of an actual robot, either through paper calculations, simulation, or experimentation.

The second portion of this thesis, Chapter 4, deals specifically with geometry relating to the task for which this particular robot was designed. Another avenue of future work would be to apply this idea of jamming states and prevention monitors to other applications. For instance, a similar heavy lift robot used on an off shore oil rig to lift and connect pipe sections would have significantly different jamming conditions than square connectors sliding through square slots. Each new application may require significant preliminary investigation of part geometry and jamming states, but once this initial work is performed the resulting system can leverage the jam prevention architecture presented in this thesis.

1.   Adams, Jeffrey D. and Daniel E. Whitney. "Application of Screw Theory to Constraint Analysis of Assemblies of Rigid Parts." IEEE International Symposium on Assembly and Task Planning. 1999. 69-74.

2.   An, Chae H. and John M. Hollerbach. "Dynamic Stability Issues in Force Control of Manipulators." IEEE. 1987. 890-896.

3.   Bruyninckx, H., S. Dutre, and J. DeSchutter. "Peg-on-Hole: A Model based Solution to Peg and Hole Alignment." IEEE International Conference on Robotics and Automation. 1995. 1919-1924.

4.   Caine, Michael E., Tomas Lozano-Perex, and Warren P. Seering. "Assembly Strategies for Chamferless Parts." IEEE. 1989. 472-477.

5.   Carignan, Craig R. and David L. Akin. "Using Robots for Astronaut Training." IEEE Control Systems Magazine. 2003. 46-59.

6.   Colgate, Ed and Neville Hogan. "An Analysis of Contact Instability in Terms of Passive Physical Equivalents." IEEE. 1989. 404-409.

7.   Dayan, Joshua, Min Zou and Itzhak Green. "Contact Elimination in Mechanical Face Seals using Active Control." IEEE Transactions on Control Systems Technology, Vol 10, No 3. 2002. 344-354.

8.   Dohring, Mark and Wyatt S. Newman. "The Passivity of Natural Admittance Control Implementations." IEEE International Conference on Robotics and Automation. 2003. 3710-3715.

9.   Eppinger, Steven D. and Warren P. Seering. "Introduction to Dynamic Models for Robot Force Control." IEEE Control Systems Magaine. 1987. 48-52.

10. Eppinger, Steven D. and Warren P. Seering. "Three Dynamic Problems in Robot Force Control." IEEE Transactions on Robotics and Automation, Vol 8, No 6. 1992. 751-758.

11. Eppinger, Steven D. and Warren P. Seering. "Understanding Bandwidth Limitations in Robot Force Control." IEEE. 1987. 904-909.

12. Fasse, Ernest D. and Jan F. Broenink. "A Spacial Impedance Controller for Robotic Manipulation." IEEE Transactions on Robotics and Automation, Vol 13, No 4. 1997. 546-556.

13. Fetherstone, Roy and Stef Sonck and Oussama Khatib. "A General Contact Model for Dynamically-Decoupled Force/Motion Control."

14. Friedland, B. and Y. Park. "On Adaptive Friction Compensation." IEEE Transactions on Automatic Control, Vol. 37, Issue 10, pp. 1609-1612, October 1992.

15. Garretson, Justin. "High-Precision Control of a Heavy-Lift Manipulator in a Dynamic Environment." Master's Thesis. Mechanical Engineering Dept. Massachusetts Institute of Technology. 2005.

16. Glosser, Gregory D. and Wyatt S. Newman. "The Implementation of a Natural Admittance Controller on an Industrial Manipulator." IEEE. 1994. 1209-1215.

17. Hogan, N. "Impedance Control of Industrial Robots." Robotics & Computer-Integrated Manufacturing. 1984. Vol 1, No 1. 97-113.

18. Hogan, N. "Impedance Control: An Approach to Manipulation: Part 1-Theory." Journal of Dynamic Systems, Measurement and Control. 1985, Vol 107. 1-7.

19. Hogan, N. "Impedance Control: An Approach to Manipulation: Part 2-Implementation." Journal of Dynamic Systems, Measurement and Control. 1985, Vol 107. 8-16.

20. Hogan, N. "Impedance Control: An Approach to Manipulation: Part 3-Applications." Journal of Dynamic Systems, Measurement and Control. 1985, Vol 107. 17-24.

21. Hogan, N. "On the Stability of Manipulators Performing Contact Tasks." IEEE Journal of Robotics and Automation, Vol 4, No 6. 1988. 677-686.

22. Hogan, Neville. "Stable Execution of Contact Tasks Using Impedance Control." IEEE. 1987. 1047-1054.

23. Huang, Shuguang and Joseph M. Schimmels. "Sufficient Conditions Used in Admittance Selection for Planar Force-Guided Assembly." IEEE International Conference on Robotics and Automation. 2002. 538-543.

24. Huang, Shuguang and Joseph M. Schimmels. "Sufficient Conditions Used in Admittance Selection for Force-Guided Assembly of Polygonal Parts." IEEE Transactions of Robotics and Automation, Vol 19, No 4. 2003. 737-742.

25. Huang, Shuguang and Joseph M. Schimmels. "The Eigenscrew Decomposition of Spatial Stiffness Matricies." IEEE Transactions on Robotics and Automation, Vol 6, No 2. 2000. 146-156.

26. Jacobsen, S. C., I. D. McCammon, K. B. Biggers, and R. P. Phillips. "Tactile Sensing System Design Issues in Machine Manipulation." IEEE. 1987. pp 2087-2096.

27. Kazerooni, H. "Contact Instability of the Direct Drive Robot when Constrained by a Rigid Environment." IEEE Transactions on Automatic Control. 1990. 710-714.

28. Kazerooni, H. "Extenders: Human Machien Interaction via the Transfer of Power and Information Signals." IEEE International Workshop on Intelligent Robots and Systems Programs. 1988. pp 737-742.

29. Kazerooni, H. and Ming-Guo Her. "The Dynamics and Control of a Haptic Interface Device." IEEE Transactions on Robotics and Automation, Vol 10. No 4. 1994. pp 453-464.

30. Kazerooni, H. and S. L. Mahoney. "Dynamics and Control of Robotic Systems Worn by Humans." IEEE International Conference on Robotics and Automation. 1991. pp 2399-2405.

31. Kazerooni, H., Tsing-luan Tsay, and Karin Hollerbach. "A Controller Design Framework for Telerobotic Systems." IEEE Transactions on Control Systems Technology, Vol 1, No 1. 1993. pp 50-62.

32. Kittipongpattana, T. and D. Laowattana. "Robotic Insertion of Dual Pegs based on Force Feedback Signals." IEEE. 1998. 527-530.

33. Lee, Sooyong and Haruhiko Asada. "Assembly of Parts with Irregular Surfaces Using Active Force Sensing." IEEE. 1994. 2639-2644.

34. Love, Lonnie J., John F. Jansen, and Francois G. Pin. "Compensation of Wave-Induced Motion and force Phenomena for Ship-Based High Performance Robotic and Human Amplifying Systems." Oak Ridge National Laboratory Technical Report. October, 2003.

35. Matko, Drago, Roman Kamnik, and Tadej Bajd. "Adaptive Impedance Control of the Industrial Robot." 46.

36. Meggiolaro, Marco A., Peter C. L. Jaffe, and Steven Dubowsky. "Achieving Fine Absolute Positioning Accuracy in Large Powerful Manipulators." IEEE International Conference on Robotics and Automation. 1999. 2819-2824.

37. Moosavian S. Ali A. and Evangelos Papadopoulos. "Multiple Impedance Control for Object Manipulation." IEEE International Conference on Intelligent Robots and Systems. 1998. 1-6.

38. Morris, Daniel M., Ravi Hebbar, and Wyatt S. Newman. "Force Guided Assemblies Using a Novel Parallel Manipulator." IEEE International Conference on Robotics and Automation. 2001. 325-330.

39. Newman, Wyatt S., M. Branicky, H. Podgurski, S. Chhatpar, L. Huang, J. Swaminathan, and H. Zhang. "Force-Responsive Robotic Assembly of Transmission Components." IEEE International Conference on Robotics and Automation. 1999. 2096-2102.

40. Pfeffer, Lawrence, Oussama Khatib, and John Hake. "Joint Torque Sensory Feedback in the Control of a PUMA Manipulator." IEEE Transactions on Robotics and Automation, Vol 5, No 4. 1989. 418-425.

41. Schimmels, Joseph M. "A Linear Space of Admittance Control Laws that Guarantees Force-Assembly with Friction." IEEE Transactions on Robotics and Automation, Vol 13, No 5. 1997. 656-667.

42. Schimmels, Joseph M. and Michael A. Peshkin. "Admittance Matrix Design for Force-Guided Assembly." IEEE TRansations on Robotics and Automation, Vol 8, No. 2. 1992. pps 213-227.

43. Schimmels, Joseph M. and Michael A. Peshkin. "Force-Assemblability: Insertion of a Workpiece into a Fixture Guided by Contact Forces Alone." IEEE International Conference on Robotics and Automation. 1991. pps 1296-1301.

44. Schimmels, Joseph M. and Michael A. Peshkin. "Force-Assembly with Friction." IEEE Transactions on Robotics and Automation, Vol 10, No 4. 1994. 465-479.

45. Schimmels, Joseph M. and Michael A. Peshkin. "The Space of Admittance Control Laws that Guarantees Force-Assembly with Friction." IEEE. 1993. 443-448.

46. Schneider, Stanlet A. and Robert H. Cannon Jr. "Object Impedance Control for Cooperative Manipulation: Theory and Experimental Results." IEEE Transactions on Robotics and Automation. 1992. 383-394.

47. Sciavicco, L. and B. Siciliano. "Modeling and Control of Robot Manipulators." Springer. London. 2000.

48. Seraji, Homayoun and Richard Colbaugh. "Adaptive Force-Based Impedance Control." IEEE International Conference on Intelligent Robots and Systems. 1993. 1537-1544.

49. Seraji, Homayoun. "Adaptive Admittance Control: An Approach to Explicit Force Control in Compliant Motion." IEEE. 1994. 2705-2712.

50. Sharon, Andre and Neville Hogan and David E. Hardt. "High Bandwidth Force Regulation and Inertia Reduction using a Macro/Micro Manipulator." IEEE. 1988. 126-132.

51. Simunovic, Sergio N. "Task Descriptors for Automated Assembly." Master's Thesis. Mechanical Engineering Dept. Massachusetts Institute of Technology. 1976.

52. Smith, Fraser, Stephen Jacobsen, Kent Backman, and Klaus Biggers. "High Dexterity, Force Reflective Telerobot for Subsea Applications." IEEE. 1991.

53. Snyder, Tanya J. and H. Kazerooni. "A Novel Material Handling System." IEEE International Conference on Robotics and Automation. 1996. pp 1147-1152.

54. Sturges, R. H. and Schitt Laowattana. "Virtual Wedging in Three Dimensional Peg Insertion Tasks." IEEE International Conference on Intelligent Robots and Systems. 1992. 1295-1302.

55. Tan, Kok Leong. "Intelligent Assist Device: Design and Development." 4th National Conference on Telecommunication Technology Proceedings, Shah Alam, Malaysia. 2003. pp. 198-202.

56. Volpe, Richard and Pradeep Khosla. "A Theoretical And Experimental Investigation of Explicit Force Control Strategies for Manipulators." IEEE Transactions on Automatic Control, Vol 38, No 11. 1993. 1624-1650.

57. Volpe, Richard and Pradeep Khosla. "Analysis and Experimental Verification of a Fourth Order Plant Model for Manipulator Force." IEEE Robotics and Automation Magazine. 1994. 4-13.

58. Waibel, Brian J. and H. Kazerooni. "Theory and Experiments on the Stability of Robot Compliance Control." IEEE Transactions on Robotics and Automation, Vol 7, No 1. 1991. 95-104.

59. Whitney, Daniel E. "Quasi-Static Assembly of Compliantly Supported Rigid Parts." ASME Journal of Dynamic Systems, Measurement and Control. 1982. pp. 65-77.

60. Yamashita, T., I. Godler, Y. Takahashi, K. Wada, and R. Katoh. "Peg-and-hole Task by Robot with Force Sensor: Simulation and Experiment." IEEE IECON. 1991. 980-985.

APPENDIX

A

TASK SPECIFICATIONS

To provide specifications for the insertion task, a description of the geometry and mass parameters of the payload and all geometry of the mating parts is required.

The payload carried by the end-effector of the robot during the "complex insertion task" for the insertion task consists of a large, 156kg cylinder with three attachment lugs. The overall dimensions and locations of these three lugs are shown in Figure A.1.
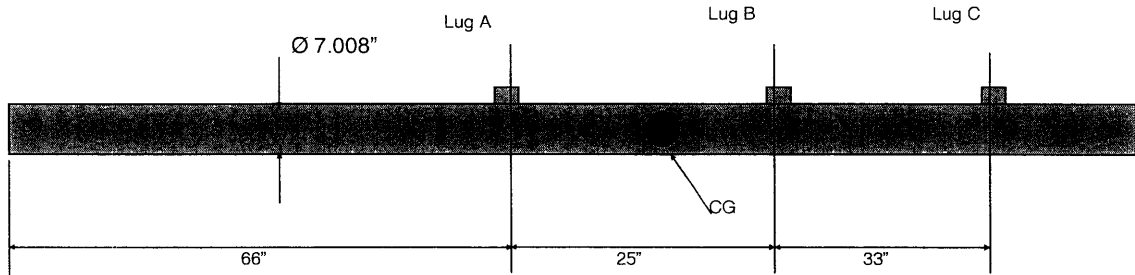
Figure A.1: Overall payload dimensions

The task to be performed involves moving the payload up flush with the environment where all three lugs will simultaneously engage with their corresponding mating locations. This initial insertion clears the lugs into the entrance of a channel. A

transverse motion 10cm down this channel is required to lock the payload into place. This motion is illustrated in Figure A.2.
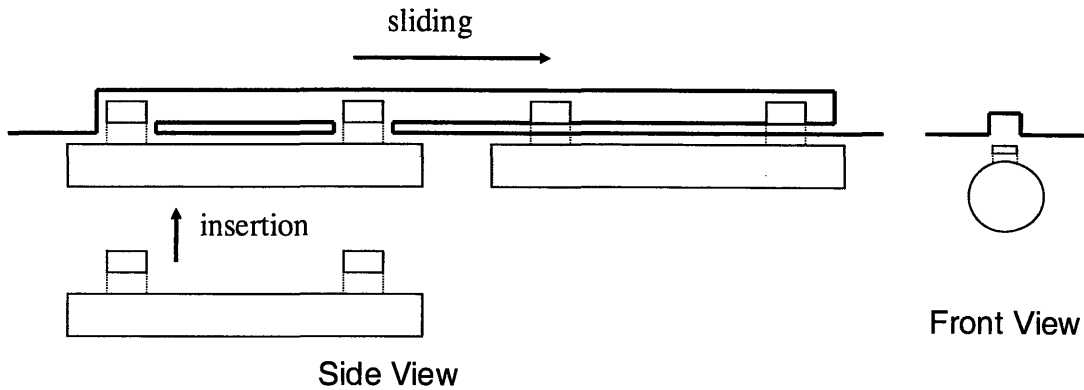
sliding

insertion

Side View

Front View

Figure A.2: Motion description for complex insertion task

A top view of the lugs and their corresponding connection points is show in Figures A.3 and A.4. Note that the fore and aft lugs on the payload are identical and consist of a square connector mating with a square hole in the environment. The central connector
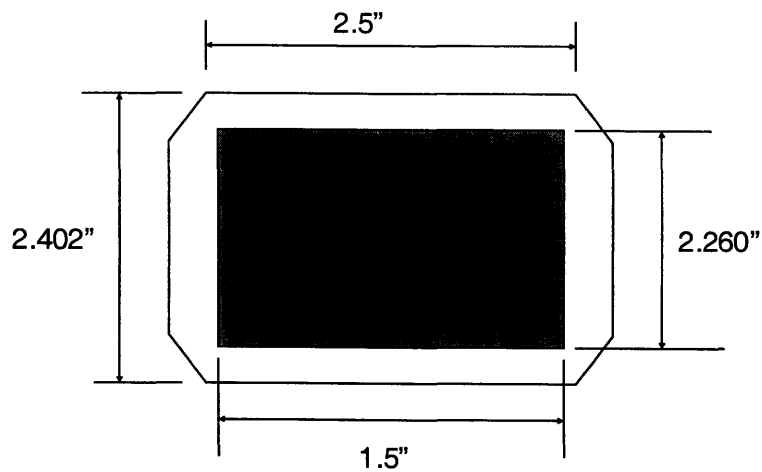
2.5"

2.402"

2.260"

1.5"

Figure A.3: Dimensions for lugs A and C and corresponding mating part

consists of an external mating where the lug mates around the outside of a corresponding feature in the environment. Most contacts will occur at the exterior contact points (the front of the forward lug and the rear of the aft lug) so it is not expected that the dimensions of the internal lug will be of any consequence on the final system.
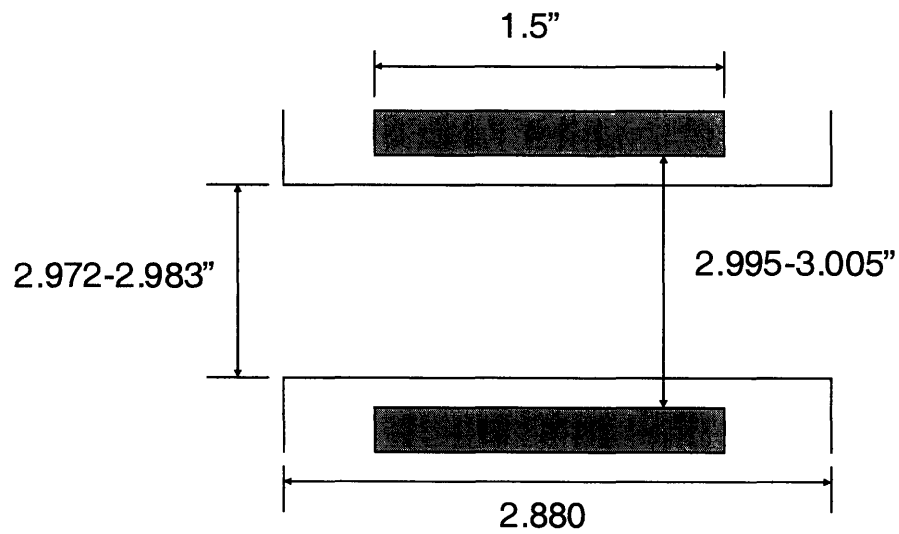

Figure A.4: Dimensions for lug B and corresponding mating part

The linear displacement allowable for these lugs is illustrated by Figure A.5 and consists of part tolerances and chamfer widths. This is also outlined in Equation A.1:

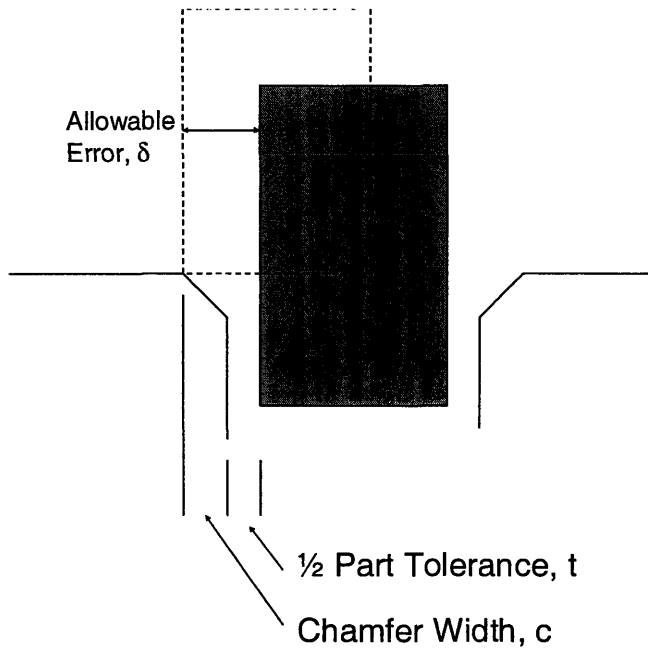$$\delta = c + t \qquad\qquad (A.1)$$

Figure A.5: Linear tolerance calculation

Given the linear displacement tolerances at the front and rear lugs it is possible to calculate the allowable yaw angle which will adhere to these constraints on the front and rear lug. These calculations are shown in Figure A.6 and equated in Equation A.2.

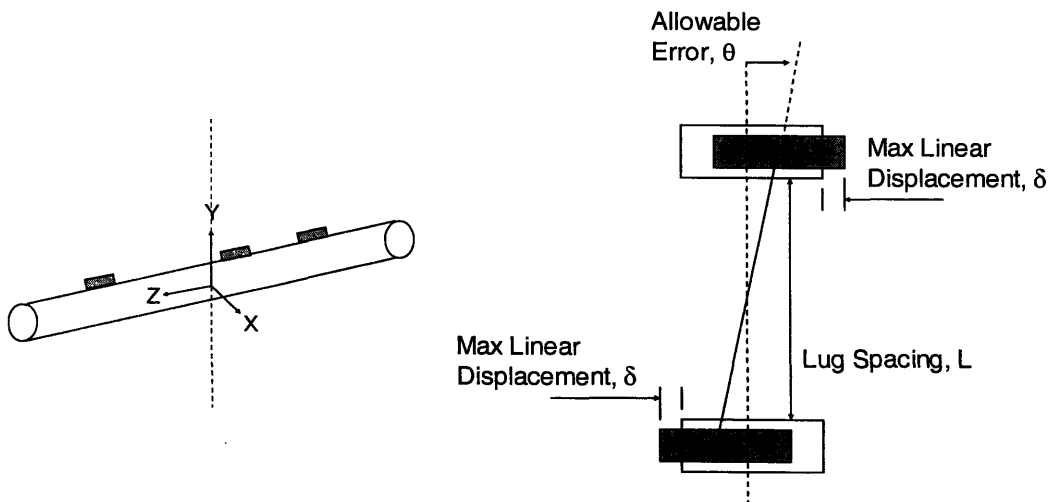$$\theta = \tan^{-1}(\frac{\delta}{1/2 \cdot L})$$ (A.2)

Figure A.6: Yaw tolerance calculation

Allowable angles for pitch displacement are established by requiring all lugs to engage simultaneously. For this to occur, if the front lug is completely engaged, the rear lug must be beginning its engagement. This is illustrated in Figure A.7 and the resulting tolerance, calculated from the lug height, is shown in Equation A.3.
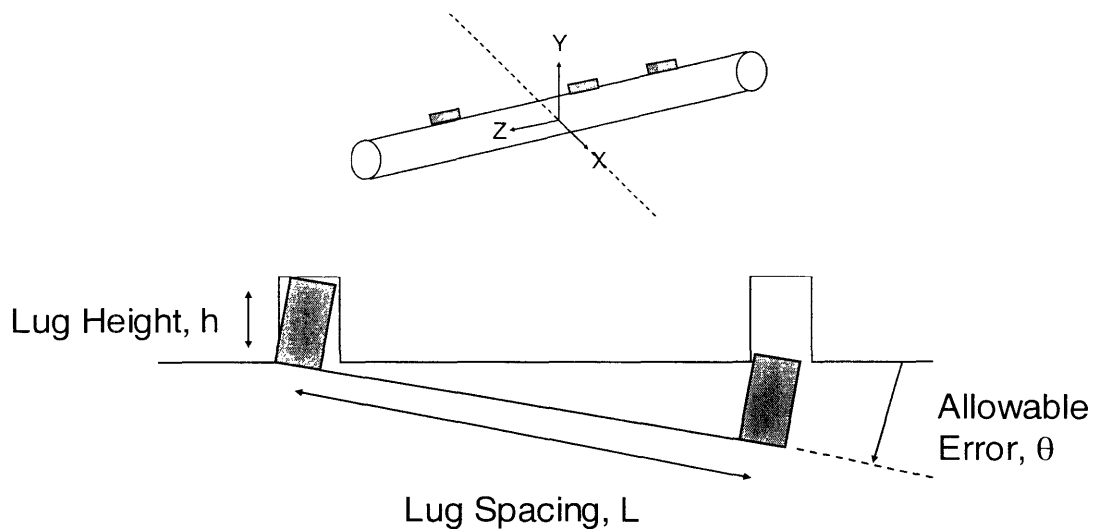
$$\theta = \tan^{-1}(\tfrac{h}{L})$$ (A.3)

Figure A.7: Pitch tolerance calculation

Allowable roll angles are calculated only from the wedging condition discussed in chapter 4 and references direction to Whitney [59]. This tolerance is illustrated in Figure A.6 and calculated in Equation A.4. For the cause of our particular task, the wedging angular tolerance is significantly larger than the pitch and yaw tolerances calculated above. As such, it will likely not represent a serious constraint on the final system.

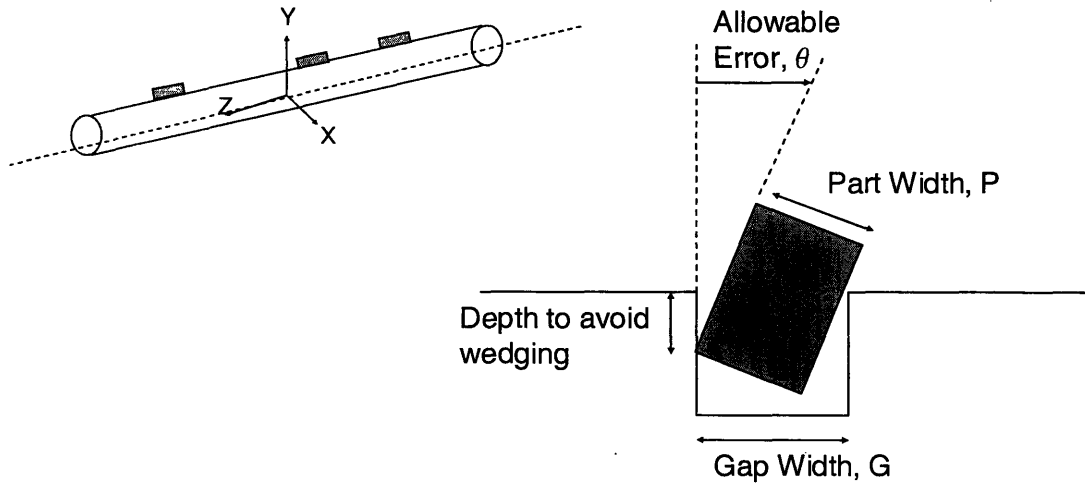$$\theta = \frac{(G - P)/G}{\mu} \qquad\qquad (A.4)$$

Figure A.8: Roll tolerance calculation

The final task specifications are listed in Table A.1.

Direction	Allowable Error
ΔX	2.3-2.8mm
ΔZ	2.54 cm
θX (pitch)	0.5 deg
θY (yaw)	0.14 deg
θZ (roll)	2.4-5.6 deg

Table A.1: Final part tolerance specifications

B

ENVIRONMENT MODEL

This appendix contains the details of the model described for testing force controller design discussed in Chapter 2. For clarity, this model is repeated in Figure B.1. Parameters used in this analysis are listed in Table B.1.

Name		Value
Robot	Robot Mass (M_R)	697 kg
	Robot Stiffness (K_R)	0 N/m
	Robot Damping (B_R)	5×10^4 Ns/m
Sensor	Sensor Mass (M_S)	1 kg
	Sensor Stiffness (K_S)	5×10^6 N/m
	Sensor Damping (B_S)	5×10^3 Ns/m
Gripper/Payload	Payload Mass (M_P)	156 kg
	Gripper Stiffness (K_C)	5.5×10^5 N/m
	Gripper Damping (B_C)	5×10^3 Ns/m
Environment	Environment Stiffness (K_E)	2.75×10^6 N/m
	Environment Damping (B_E)	5×10^3 Ns/m

Table B.1: Environment/robot interaction model parameters used in analysis

The goal is to determine transfer functions for both output environmental force and output robot position based on the one input: actuator force F. A state space model is derived and a commercial computer package (MATLAB, etc.) is used to extract the desired transfer functions. The state vector for this model is the vector of mass positions and mass velocities, shown in Equation B.1.

$$\vec{X} = \begin{bmatrix} X_R \\ X_S \\ X_P \\ V_R \\ V_S \\ V_P \end{bmatrix} \tag{B.1}$$

To derive equations of motion for this system, it is straightforward to apply Newton's equations of motion on all three masses in the system to derive the nontrivial state equations. Performing these calculations on the presented model results in the following state space equations:

$$\dot{\vec{X}} = \begin{bmatrix} 0 & 0 & 0 & 1 & 0 & 0 \\ 0 & 0 & 0 & 0 & 1 & 0 \\ 0 & 0 & 0 & 0 & 0 & 1 \\ \dfrac{-(K_R+K_S)}{M_R} & \dfrac{K_S}{M_R} & 0 & \dfrac{-(B_R+B_S)}{M_R} & \dfrac{B_S}{M_R} & 0 \\ \dfrac{K_S}{M_S} & \dfrac{-(K_S+K_C)}{M_S} & \dfrac{K_C}{M_S} & \dfrac{B_S}{M_S} & \dfrac{-(B_S+B_C)}{M_S} & \dfrac{B_C}{M_S} \\ 0 & \dfrac{K_C}{M_P} & \dfrac{-(K_C+K_P)}{M_P} & 0 & \dfrac{B_C}{M_P} & \dfrac{-(B_C+B_P)}{M_P} \end{bmatrix} \cdot \vec{X} + \begin{bmatrix} 0 \\ 0 \\ 0 \\ \dfrac{1}{M_R} \\ 0 \\ 0 \end{bmatrix} \cdot F \tag{B.2}$$

$$\begin{bmatrix} X_R \\ F_C \end{bmatrix} = \begin{bmatrix} 1 & 0 & 0 & 0 & 0 & 0 \\ K_S & -K_S & 0 & 0 & 0 & 0 \end{bmatrix} \cdot \vec{X} + \begin{bmatrix} 0 \\ 0 \end{bmatrix} \cdot F \tag{B.3}$$

The two output equations of this state space model are the robot's position and the contact force measured by the wrist sensor. These represent the feedback signals to the

inner and outer loops of the final controller, respectively. Figure B.1 illustrates the basic

controller block diagram with these two outputs modeled by the transfer functions P1 and
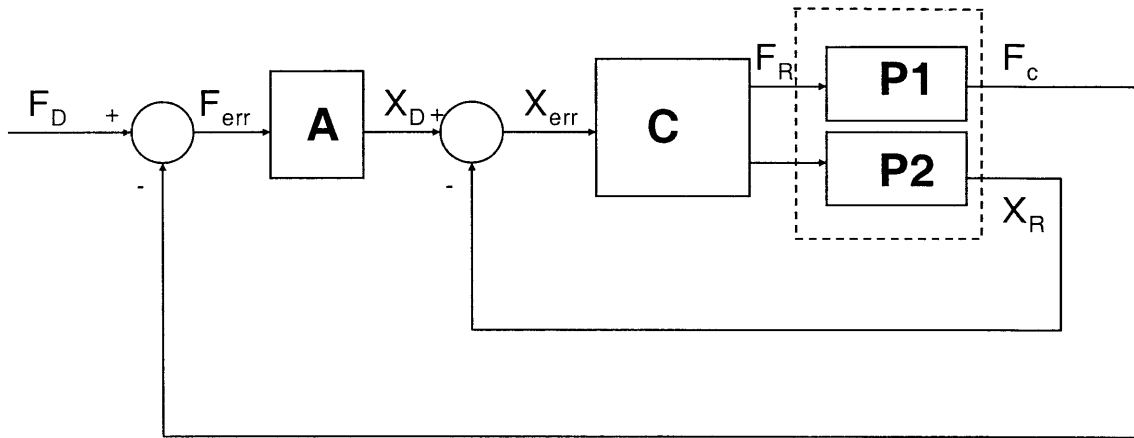
P2.

Figure B.1: Environment/robot interaction model inserted into control system block diagram

By rearranging this block diagram to the one shown in Figure B.2, the inner/outer

loop structure of the system can clearly be seen. Using P2 as the plant, the gains in the

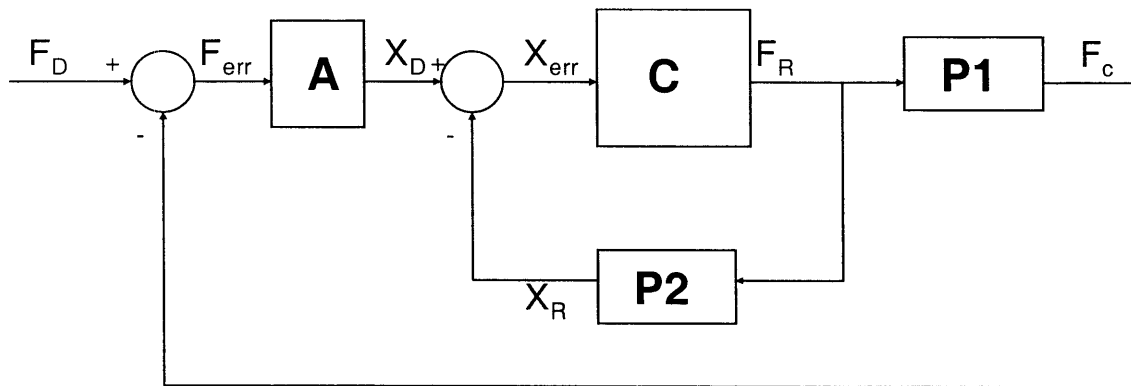position controller block, block C, can be tuned to achieve an inner loop bandwidth

Figure A.2: Rearranged control structure showing full inner/outer loop with two transfer functions

79

of .9Hz. The entire inner loop can then be reduced to one block diagram using the negative feedback reduction equation:

$$IL(s) = \frac{C(s)}{1 + P2(s) \cdot C(s)}$$

(B.4)

The behavior of the full system can then likewise be simplified by substituting IL(s) into the overall block diagram. The resulting closed loop transfer function from input (user) force to output (contact) force is then given by:

$$G(s) = \frac{A(s) \cdot IL(s) \cdot P1(s)}{1 + A(s) \cdot IL(s) \cdot P1(s)}$$

(B.5)

Desirable force following behavior is achieved by choosing a form for A(s) and choosing gains to meet the design criteria. The basic form of an A(s) admittance law discussed in Chapter 2 is repeated here as Equation B.6.

$$A(s) = K_S \cdot s + K_D + \frac{K_I}{s}$$

(B.6)